Precizna mjerenja svojstava prašine galaksija u svemiru starom 1 milijardu godina

Barišić, Ivana

Master's thesis / Diplomski rad

2016

Degree Grantor / Ustanova koja je dodijelila akademski / stručni stupanj: **University of Zagreb, Faculty of Science / Sveučilište u Zagrebu, Prirodoslovno-matematički fakultet**

Permanent link / Trajna poveznica: https://urn.nsk.hr/urn:nbn:hr:217:114701

Rights / Prava: In copyright / Zaštićeno autorskim pravom.

Download date / Datum preuzimanja: **2024-12-31**

Repository / Repozitorij:

Repository of the Faculty of Science - University of Zagreb

UNIVERSITY OF ZAGREB
FACULTY OF SCIENCE
DEPARTMENT OF PHYSICS

Ivana Barišić

Accurate measurements of the dust properties in the 1 billion year old universe

Master Thesis

Zagreb, 2016

SVEUČILIŠTE U ZAGREBU
PRIRODOSLOVNO-MATEMATIČKI FAKULTET
FIZIČKI ODSJEK

Ivana Barišić

Precizna mjerenja svojstava prašine u svemiru starom 1 milijardu godina

Diplomski rad

Zagreb, 2016

UNIVERSITY OF ZAGREB
FACULTY OF SCIENCE
DEPARTMENT OF PHYSICS

STUDY PROGRAM: Integrated Undergraduate and Graduate University Programme in Physics; Research Physics

Ivana Barišić

Master Thesis

Accurate measurements of the dust properties in the 1 billion year old universe

Advisor: Prof. Vernesa Smolčić (Physics Dept, University of Zagreb)
Co-Advisor: Dr. Peter Capak (California Institute of Technology/IPAC)

Master Thesis grade: _____

Commission: 1. _____

2. _____

3. _____

Master Thesis defence date: _____
Zagreb, 2016

I would like to express my sincere gratitude to Dr. Peter Capak for guiding me throughout this project. Thank you for all the support, motivation and shared knowledge during this learning process.
I wish to express my appreciation to Prof. Vernesa Smolčić for her support and expert advise during the project and particularly during my studies. Thank you for giving me the opportunity to learn from you.
I am especially grateful to Dr. Andreas Faisst for much useful advice, constructive critique, and many valuable discussions. Thank you for your patience, encouragement and guidance during this project.
I would like to acknowledge the Student Faculty Programs at the California Institute of Technology for giving me the opportunity to work there as an intern. Working in such a motivating environment and interacting daily with scientists and students in different research areas had an influence on me and extended my knowledge horizons.

Precizna mjerenja svojstava prašine u svemiru starom 1 milijardu godina

Sažetak

U ovom radu proučavam svojstva atenuacije prašine 11 galaksija, sa prosječnim stupnjem formiranja novih zvijezda, na crvenom pomaku $5 < z < 6$ u COSMOS polju koristeći *Hubble Space Telescope* Wide Field Camera 3 (HST WFC-3) podatke visoke rezolucije u ultaljubičastom dijelu spektra u sustavu mirovanja galaksija. Također, koristim podatke u daleko - infracrvenom (FIR) kontinuumu i [CII] emisijske linije opažene sa Atacama Large Millimeter Array (ALMA). U prijašnjem radu za isti skup galaksija, gdje koriste podatke niskog omjera signala - prema - šumu pronađeno je da ove galaksije imaju veće vrijednosti ultraljubičastih (UV) spektralnih nagiba za fiksne vrijednosti omjera FIR i UV luminoziteta, u odnosu na galaksije u lokalnom svemiru. Ta razlika je mogla biti uzrokovana sistematskim efektima u mjerenjima infracrvenog luminoziteta i UV spektralnih nagiba, ili pak promjenama u geometriji prašine ili dinamici u galaksijama na visokom crvenom pomaku. Koristeći podatke visokih omjera signal - prema - šumu dobila sam konzistentne UV spektralne nagibe sa vrijednostima dobivenim u prijašnjem radu. Ovaj rezultat pokazuje da se razlika između galaksija na visokom i niskom crvenom pomaku može pripisati drugačijim svojstvima prašine i plina u galaksijama na visokom crvenom pomaku ($z > 5$). No, sa mojim novim mjerenjima i dodatnim testovima njihove pouzdanosti i preciznosti, zaključujem da dio galaksija na visokom crvenom pomaku pokazuje slična svojstva prašine galaksijama na niskom crvenom pomaku. Unatoč tome, to nije slučaj za podskup mog seta galaksija koje pokazuju vrlo niske omjere FIR prema UV luminozitetima, ukazujući tako na drugačija svojstva plina i prašine prisutna u tim galaksijama.

Accurate measurements of the dust properties in the 1 billion year old universe

Abstract

In this work I examine the dust attenuation properties of 11 average star-forming galaxies at high redshift $5 < z < 6$ in the COSMOS field using deep high resolution rest-frame ultraviolet (UV) *Hubble Space Telescope* Wide Field Camera 3 (HST WFC-3) data along with far - infrared (FIR) continuum and [CII] emission line measurements from the Atacama Large Millimeter/Submillimeter Array (ALMA). In the previously conducted study of the same sample of galaxies, using low signal-to-noise ground based telescope data, it was found that these galaxies have higher dust column densities, i.e. redder UV continuum slopes, at a fixed FIR to UV luminosity ratio, compared to the average of local galaxies. This apparent difference is either caused by systematic measurement biases in the infrared luminosity and ultraviolet slope estimates, or changes in dust geometry or gas dynamics in high redshift galaxies. With the high signal-to-noise HST WFC-3 data I find mainly consistent UV continuum slope values compared to the ones from the low signal-to-noise ground based data. This result shows that differences between galaxies at low and high redshift found in previous studies are due to different dust and gas properties in high redshift ($z > 5$) galaxies. With HST WFC-3 measurements and additional tests of their reliability and accuracy, I conclude that some of the high redshift galaxies show similar dust attenuation properties as low redshift galaxies. However, I find that this is not the case for the upper limit subset of our sample showing very low FIR to UV luminosity ratios, hinting towards different dust and gas properties.

Table of contents

1 INTRODUCTION

1.1 Thesis overview

It is important to study physical properties of galaxies at high redshift as it allows us to see how galaxies evolve through cosmic time. In particular, I study dust properties of a set of Lyman-break galaxies in the 1 billion year old universe to investigate their metallicities and star-formation rates (SFRs).

The ultraviolet emission from young and hot stellar populations in galaxies often suffers from dust extinction. The consequence of this effect is that the total SFR of a galaxy can not be only measured from the observed ultraviolet (UV) emission. Infrared (IR) emission coming from dust grains heated by absorption of the UV radiation is used to find the SFR in IR. The total SFR is then found by adding the IR SFR to the UV SFR. The rest-frame IR emission at high redshift galaxies often can not be probed due to limitations of current instruments to cover longer wavelengths to which rest-frame IR emission is shifted. The dust extinction is then estimated from the infrared excess, and the dust column density β (i.e. amount of the dust along the line-of-sight) from flux density measurements in the rest-frame UV of the galaxy. Using a tight correlation between the infrared excess and dust column density β one can determine UV flux density re-radiated by dust in the IR. Knowing the total star-formation rate we can better understand the cosmic star formation history.

In the following section I give a brief introduction to the general process of SFR in galaxies, Lyman-break galaxies, and how dust can affect measurements and what models are being used to correct for the dust extinction in observed galaxies. In Section 2, I give an overview of the field in which a set of 11 Lyman-break galaxies studied in this work have been observed, about the instruments used for their observation, as well as an overview of the dataset used in this work. In Section 3, I describe methods that I used to analyze the dataset, and describe how I performed the analysis. The results of this work and discrepancies with previous work are described in Section 4. In Section 5, I discuss the results of this work, while in Section 6 I give the summary of this work and an overview of future work.

1.2 Star-formation rate

Galaxies differ in their shape and size. Likewise, they differ in the rate at which they form new stars in a certain time frame, the so-called SFR. The SFR changes dramatically during the lifetime of a galaxy, and the processes that are responsible for its change are still being studied. Other than in the local universe, it is difficult to measure star-formation directly at higher redshifts, because current instruments limit the long wavelength measurements which cover the rest-frame far-infrared (FIR) emission from high redshift galaxies [19]. The SFR can be measured by UV and FIR continuum emission and emission lines.

Even though stellar populations produce light over a broad range of wavelengths, the observed UV luminosity of a galaxy is mostly coming from UV radiation from short lived, young and massive stellar populations. The UV luminosity is highly influenced by the metallicity of the stars, i.e. more metal rich stars tend to emit less UV light [18]. Metallicity of stars in a galaxy is influenced by the star-formation history, and stellar metallicities play important role for the observed ultraviolet luminosity.

The SFR in the UV is determined from the UV radiation coming from young, hot and massive stellar populations, however, it does not correspond to the total SFR. Due to presence of the dust grains, in star-forming regions and in the interstellar medium, most of the emitting radiation from young massive stars is being absorbed and scattered. The obscuration of the emitting UV radiation by dust is rather significant, and the UV radiation needs to be corrected for the absorption effects or the absorbed energy is measured at FIR wavelengths [18].

As the UV radiation heats up the dust when it gets absorbed, the absorbed energy will be re-emitted at IR wavelengths. Thus, observing in the rest-frame IR of the galaxy it is possible to measure the absorbed UV radiation of young stars and therefore estimate the obscured SFR. This measured SFR from the IR luminosity is only a part of the total SFR, since it is coming only from radiation absorbed by dust. IR radiation from dust grains needs no correction for absorption by dust, since it is assumed that IR radiation is barely being absorbed by dust [18]. The total SFR is found by adding the SFR measured from IR radiation and the SFR measured from UV radiation which is not corrected for dust absorption.

$$SFR_{tot} = SFR_{UV} + SFR_{IR}$$

Determining the total SFR of high redshift galaxies is challenging. While the SFR_{UV} can be measured relatively easily from the rest-frame UV emission, due to current limitations of instruments, measurements of the emission in the rest-frame FIR often can not be obtained. Therefore, the UV continuum slope β is used to correct UV based SFRs to total SFRs [18].

Rest-frame optical emission lines, such as Hα, [OII], and [OIII] can as well be used to determine the SFR, e.g. out to redshift ~ 6 for the Infrared Array Camera (IRAC) above which these emission lines fall out of the wavelength coverage of this instrument. This is possible due to the link between the SFR and the photoionization rate which is a consequence of very energetic ultraviolet radiation from massive stars within galaxy [18]. Emission lines are also absorbed by dust, and require a dust correction.

The SFR of a galaxy depends on the stellar mass and on the redshift, meaning that SFR is observed to be higher in galaxies at higher redshift, and occurring earlier in more massive galaxies [21]. A tight correlation between the SFR and the stellar mass has been observed in the local universe, as well as at higher redshift up to z = 4 or higher [26]. The tight correlation of SFR - M_* at low redshifts suggests that

the main mechanism which drives the star formation in a galaxy is caused by smooth processes (e.g., gas accretion) rather than stochastic major mergers [18]. The star-forming main sequence is parametrized as SFR = M_*^{α}, where α (≈ 1) is an important measure for studying the processes that drive the mass assembly of galaxies. As found in earlier studies, α changes with redshift. Noeske et al. [21] found the parameter value of α = 0.9, while Elbaz et al. [10] found for galaxies in the local universe α = 0.77, indicating the SFR is declining with time. Daddi et al. [8] finds the value of α = 0.9 a good fit for the sample of galaxies at z = 2.

Depending on the SFR, galaxies can be roughly classified as star-forming and passive galaxies. Star-forming galaxies are active in star-formation, and it is observed at low redshifts (up to z = 2) that they follow tight SFR - M_* correlation [18, 21]. Quiescent galaxies are passive types of galaxies observed locally and at higher redshifts (up to z $\sim$ 4). Due to their quenched star-formation, they lie below the SFR - M_* correlation. Quiescent galaxies individually have no on-going star-formation in general, however, when they do form new stars their star-formation is low, and it is considered that it is driven by the process of merging [28]. Quiescent galaxies are being studied since understanding the processes that lead to suppressing their star-formation can help us understand the main question of the formation and evolution of galaxies [18].

1.3 Lyman-break galaxies

Lyman-break galaxies (LBGs) are actively star-forming galaxies, and are easy to detect at high redshifts due to the signature discontinuity in their spectral energy distribution at 912 Å . The Lyman discontinuity is a consequence of the photoelectric absorption of the ultraviolet radiation emitted by massive OB type of stars on the neutral hydrogen in the interstellar medium. Except for ionizing the neutral hydrogen, these photons are also absorbed on the gas and dust, and re-emitted in all directions. Whether or not these photons will be re-emitted from the interstellar medium, depends on the geometry of dust and gas. In case these photons manage to escape, the galaxy will appear very dim at those wavelengths [13, 27].

First LBGs were discovered at $1.5 < z < 1.8$, since they were very luminous in radio part of the electromagnetic spectrum [13]. Due to their redshift, the characteristic Lyman discontinuity at 912 Å rest-frame was shifted to optical wavelengths. The identification of their redshift was thus determined with optical telescopes.

As observed in the local universe, elliptical galaxies (i.e. early type galaxies) and bulges of spiral galaxies have low or almost no on-going star-formation and are composed of very old stellar populations. It is expected that elliptical galaxies, as well as spheroid bulges in spiral galaxies, must have formed stars earlier in cosmic time [1]. For this reason, high redshift galaxies with active star-formation, such as LBGs,

[1] http://www.astro.caltech.edu/~george/ay21/eaa/eaa-hizgals.pdf

are considered as primeval galaxies, thus studying their physical properties helps us better constrain the formation and evolution of early type galaxies.

Constraining the SFR of galaxies in the early universe allows us to make a link to the SFR of galaxies at lower redshift and in the local universe, leading to better understanding of the cosmic star formation history, and ultimately the assembly of stellar mass in galaxies across cosmic time [2]. With clustering of the LBGs we can infer the distribution of dark matter, therefore studying properties of LBGs and their environment is important in investigating the origin and properties of dark matter. However, deriving dark matter properties only from clustered LBGs may result in a bias in dark matter distribution, since dark matter in the environment of the non clustered systems might have a distribution not comparable to clustered systems.

1.3.1 Lyman α emission

Another important feature in the spectrum of a galaxy is the Lyman α emission at 1215.67 Å which originates from the transition of the atomic hydrogen from the first excited state to the ground state. This emission may occur when ionized hydrogen atom captures the electron, or when the neutral hydrogen is excited by a photon into the upper state. Either way, excited hydrogen atom then spontaneously emits the photon to transit to the ground state [14]. This emission line can also be absorbed by gas and dust, so its detection and strength of the emission line depends on the geometry of dust. It is predicted that Lyα emitting galaxies can be used to study the cosmic star-formation, as tracers of young, faint, low dust obscured actively star-forming galaxies for which the use of color selection criteria may be limited. In such young star-forming galaxies Lyα line may have narrow but high equivalent width due to low metal content if these galaxies are one of the first ones being formed [15]. As Hu et al. [15] predicts, their observation at high redshift would lead to selection of much wider population of galaxies in the early universe.

1.4 Dust in galaxies

Electromagnetic radiation from stars of all ages can be absorbed and scattered by dust within a galaxy. However, due to the size of dust grains, photons of shorter wavelengths are more likely to get absorbed and scattered [9]. Therefore, the dust grains are stochastically heated up by absorption of the electromagnetic radiation. The heating of dust is mainly dominated by the ultraviolet and optical photons from short-lived massive OB population of stars which reside in star-forming regions, called birth clouds. Presumably, a birth cloud region of galaxies is surrounded by the hydrogen gas, ionized by highly energetic photons. These photons come from short lived OB population of stars that reside within the birth cloud region. The line emission from ionized HI gas is then absorbed by the neutral hydrogen HI and in the

[2] http://www.astro.caltech.edu/~george/ay21/eaa/eaa-hizgals.pdf

surrounding interstellar medium. Birth clouds have a limited lifetime, so longer living stars manage to leave the birth cloud and their radiation heats up the dust grains in the interstellar medium. All together, the radiation absorbed by dust is re-emitted in the infrared part of the electromagnetic spectrum, according to the law of the conservation of energy [6].

Figure 1.1 from Charlot and Fall [6] is an illustration of birth cloud regions surrounded with the ionized and neutral hydrogen gas, residing within the interstellar medium. Some quantities which we are able to observe, such as flux density in this work, are to a great extent influenced by the geometry of dust in galaxy itself. The column density of dust is highly dependent on the dust geometry. There is a possibility for photons to get scattered into the line of sight, as well as out of the line-of-sight. Therefore, the measured flux density needs to be corrected for the extinction by dust. The total dust content of galaxy, called infrared excess, is independent on the dust geometry and is closely related to the dust absorption [16, 2].

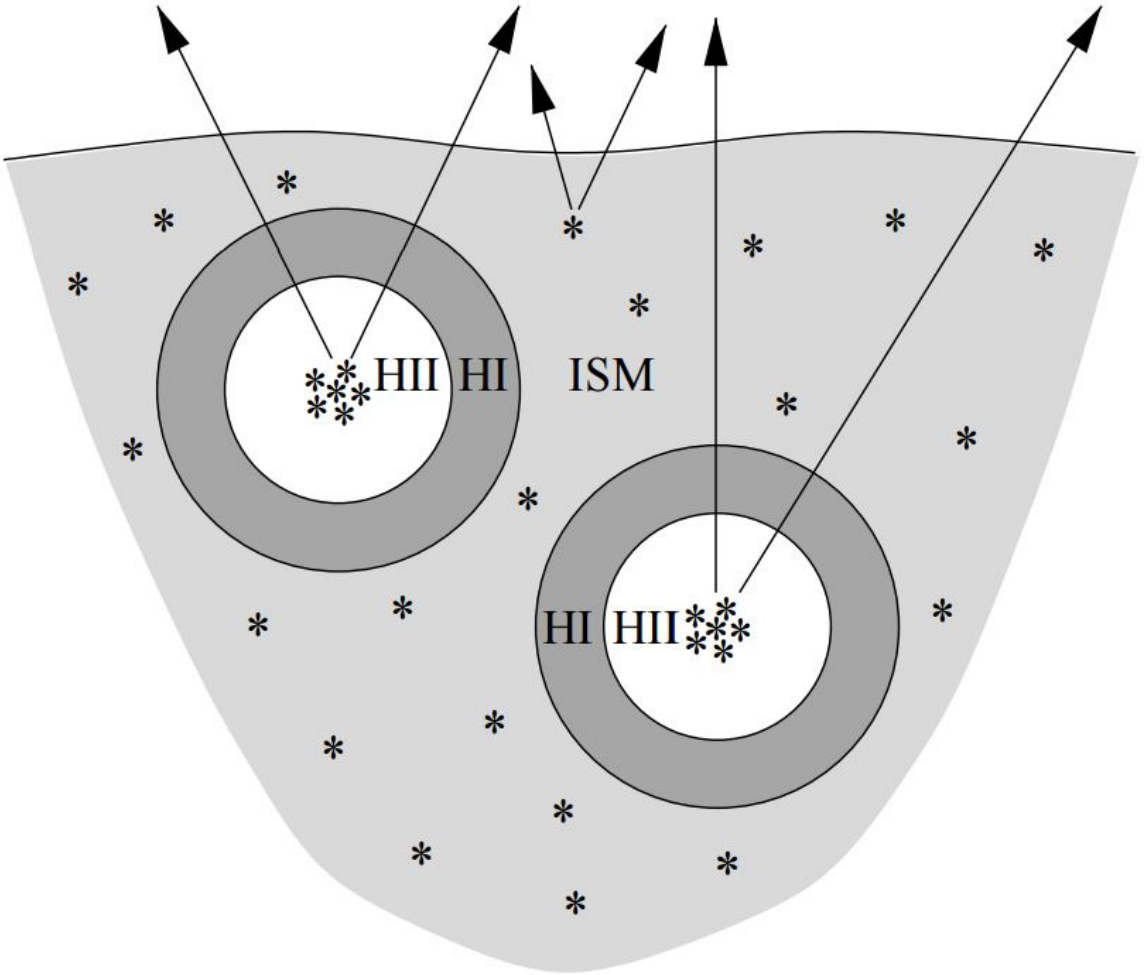

Figure 1.1: Illustration from Charlot and Fall [6] of a star-forming region within a galaxy surrounded with a hydrogen gas ionized by highly energetic photons from stars belonging to OB stellar population (white) and neutral hydrogen gas (dark grey). The interstellar medium is represented by the gray shaded area.

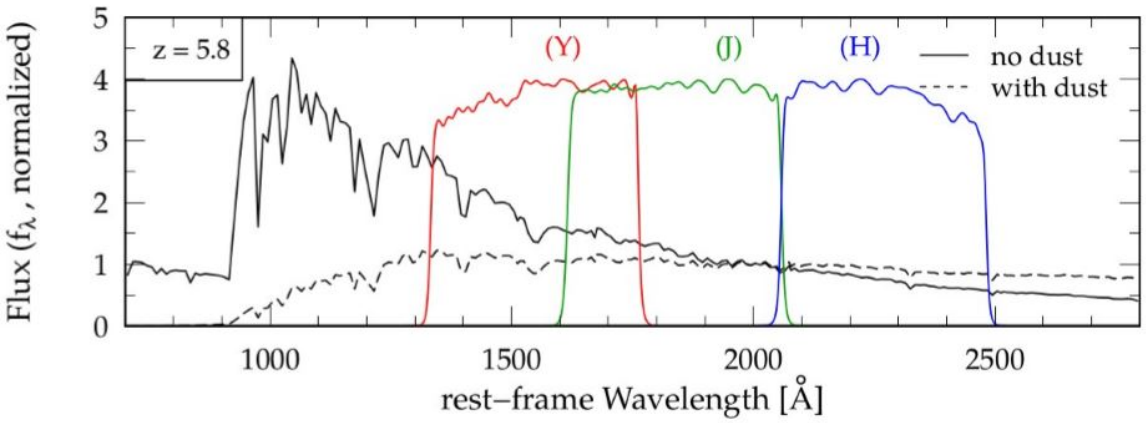

Figure 1.2: Spectral energy distribution model of a galaxy at redshift z = 5.8, with normalized flux on the y-axis and rest frame wavelength on the x-axis. If a galaxy has no dust content, its spectral energy distribution would be similar to the black curve. If galaxy has dust content, its spectral energy distribution would be similar to black dashed curve. Red (Y), green (J) and blue (H) curves represent filter coverage of various wavelength intervals, with which we observe radiation from a galaxy.

Figure 1.2 shows the spectral energy distribution model of a galaxy at redshift z = 5.8. Solid curve represents the spectral energy distribution fit for the galaxy with no dust content, and dashed curve represents the spectral energy distribution fit for the galaxy containing dust. A certain amount of flux in the ultraviolet part of the spectrum is absorbed by dust and re-emitted in the infrared part of the spectrum. This is evident in the plot from flattening of the spectral energy distribution curve of a galaxy with dust content, compared to a galaxy with no dust content. Furthermore, this provides the evidence that the column density of dust can be determined by measuring the flux density values in near - infrared bands.

Presence of the dust in a galaxy represents a major problem for observations since it can alter the flux measurements up to an order of magnitude. It is thus very important to understand the properties of dust and develop a model closest to reality to be able to correct for extinction of starlight by dust. Photons can be either absorbed by dust or scattered out of the galaxy. Therefore, luminosity from starlight unaffected by dust is given with the following relation

$$L_\lambda(t) = \overline{T}_\lambda(t) \int_0^t dt' \psi(t - t') S_\lambda(t') \tag{1.1}$$

where $\psi(t - t')$ is the SFR in the given time interval, $\overline{T}_\lambda(t)$ is the mean transmission function, and $S_\lambda(t')$ is the luminosity per unit wavelength and per unit mass by a generation of stars of age t' [6]. Photons affected by dust, the ones that get scattered and absorbed are being re-radiated in the infrared, so the luminosity of the dust is given by

$$L_{dust}(t) = \int_0^\infty d\lambda \left[1 - \overline{T}_\lambda(t)\right] \int_0^t dt' \psi(t - t') S_\lambda(t') \tag{1.2}$$

The transmission function needs to be defined as well. As mentioned earlier, when photon is emitted from the star, it passes through the birth cloud region and through the interstellar medium. Charlot and Fall [6] define the transmission function as a product of the transmission functions of birth cloud and the interstellar medium

$$T_\lambda(t, t') = T_\lambda^{BC}(t') T_\lambda^{ISM} \tag{1.3}$$

Furthermore, they define the transmission function of the birth cloud as $T_\lambda^{HII} T_\lambda^{HI}$ for $t' \leq t_{BC}$ and 1 for $t' > t_{BC}$. The transmission function of the interstellar medium they define with the following integral

$$T_\lambda^{ISM} = \int_0^\infty dt_\lambda p(\tau_\lambda) e^{-\tau_\lambda} \tag{1.4}$$

The transmission function of the interstellar medium depends on the dust geometry approximated and models used to describe the dust distribution. Using overly simplified model such as uniform dust distribution within galaxy leads to uncertainties in determining the physical properties of galaxies [6]. Charlot and Fall [6] developed a model in which they describe the absorption of the radiation from stars by dust and give three ideal types of dust distribution in the interstellar medium. These types are namely foreground screen, mixed slab and discrete clouds.

Foreground screen considers the uniform dust distribution in front of the stars, which is as mentioned before an oversimplified model, and absorbs electromagnetic radiation equally from all stars [6].

$$\begin{aligned} p(\tau_\lambda) &= \delta(\tau_\lambda - \tau_\lambda^{sc}) \\ T_\lambda^{ISM} &= exp(-\tau_\lambda^{sc}) \end{aligned} \tag{1.5}$$

Where τ_λ is the optical depth of absorption of the photon, τ_λ^{sc} is the optical depth of the screen, $p(\tau_\lambda)$ is the probability of the optical depth τ_λ, and T_λ^{ISM} is the transmission function of the interstellar medium.

Mixed slab is a type of dust distribution which considers that stars, as sources of radiation, and the interstellar medium are uniformly mixed.

$$\begin{aligned} p(\tau_\lambda) &= 1/2\tau_\lambda^{sl}, \qquad for \quad \tau_\lambda \leq \tau_\lambda^{sl} \\ p(\tau_\lambda) &= \tau_\lambda^{sl}/2\tau_\lambda^2, \qquad for \quad \tau_\lambda > \tau_\lambda^{sl} \\ T_\lambda^{ISM} &= \frac{1}{2\tau_\lambda^{sl}} \left[1 + \left(\tau_\lambda^{sl} - 1\right) exp\left(-\tau_\lambda^{sl}\right) - \left(\tau_\lambda^{sl}\right)^2 E_1\left(\tau_\lambda^{sl}\right)\right] \end{aligned} \tag{1.6}$$

where E_1 is the exponential integral of the first order and τ_λ^{sl} is the optical depth of the mixed slab [6].

Third type of the dust distribution in the interstellar medium, and to date most realistic model used in many recent studies, considers clumpy distribution of dust, where clumps of dust are non-uniformly distributed themselves and vary in shape and size. Optical depth probability and the transmission function are defined as following

$$
\begin{aligned}
p\left(\tau_\lambda\right) &= \sum_{n=0}^{\infty} \frac{\overline{n}^n}{n!} exp\left(-\overline{n}\right) \delta\left(\tau_\lambda - n\tau_\lambda^c\right) \\
T_\lambda^{ISM} &= exp\left[-\overline{n}\left(1 - e^{-\tau_\lambda^c}\right)\right]
\end{aligned}
\tag{1.7}
$$

where τ_λ^c is the optical depth of the cloud, while $\overline{n}$ is the mean number of clouds on the path of the photon. Probability for a photon to encounter a certain optical depth has been approximated with a Poisson distribution [6]. As some previous works stated [7, 4] the observed emission from galaxies in infrared part of the spectrum comes from three main different dust components. These dust components are hot grains, warm grains and polycyclic aromatic hydrocarbons.

1.4.1 Hot dust

These dust grains are smaller than 0.01 μm in size. As stated by Purcell [23], the temperature of these grains in the thermal equilibrium would be between 10 - 15 K due to the interstellar radiation field, in case they had large heat capacity. Furthermore, as a consequence of having low heat capacity, the time needed for these grains to cool off happens to be shorter than the interval of absorbing a new photon [23]. Due to their low heat capacity they can have a broad range of temperatures, which can be order of magnitude from 10 K to 1000 K. These dust grains are therefore stochastically heated up. They are considered as additional contributors to the continuum emission in mid-infrared along with the polycyclic aromatic hydrocarbon molecules.

1.4.2 Warm dust

Warm dust is considered as dust grains of size between 0.01 and 0.25 μm [7]. These grains are considered to be big in size, compared to hot dust grains. Due to their size they continuously absorb photons or scatter them so since they have not enough time to cool between two incident high energetic photons it can be approximated that they are in the state of thermal equilibrium [9].

1.4.3 Cold dust

Cold dust are considered to be dust grains with temperatures lower then T $<$ 10 K [3]. These grains can be modeled as a modified black body, however, this type of modeling

[3] https://ned.ipac.caltech.edu/level5/March05/Li/Li5.html

results in overestimate of cold dust temperature. This is because the emission from cold dust grains is in such wavelength range it can interfere with the emission from warm dust grains (24 - 70 μm) [12]. The process which leads to heating of the cold dust grains is still being studied.

1.4.4 PAH molecules

The polycyclic aromatic hydrocarbon (PAH) molecules are considered to be the main contributors to the continuum emission in mid-infrared part of the electromagnetic spectrum. From studies of Milky Way and nearby galaxies it has been observed that PAH molecules reside in regions of galaxies with either active or recently active star-formation. These molecules, mostly carbonaceous, are only a few Å in diameter. They are excited to higher energy levels by absorbing the UV and optical photons, and is predicted they reside in outer parts of the HII regions, between the ionized and neutral gas. By absorbing these highly energetic photons, they emit photoelectrons, which can heat up the interstellar gas [29]. However, their presence in galaxies at redshift $z > 3$ is still a being studied [25].

2 INSTRUMENTS AND DATASET

Electromagnetic waves of wavelengths shorter than ultraviolet are energetic enough to ionize atoms and molecules in the Earth's atmosphere, so this radiation does not pass through to the ground. Figure 2.1 shows the atmospheric transmission as a function of wavelength. It is evident that the atmosphere is transparent to radio waves, and to visible light. Even though the atmosphere is transparent for most of the visible light, some of the photons do get absorbed by molecules in the atmosphere. This is a disadvantage for ground based optical telescopes. Also, ground based optical telescopes are being limited by the time of the day in which observations can be performed. Additionally, there are limitations related to atmospheric effects, i.e. seeing, which can alter the electromagnetic radiation from the source of the interest.

Over the years instrumentation and telescopes have been improved and therefore the quality of ground based observations at optical wavelengths became better. Still, observations of objects at high redshifts ($z > 3$) by ground based telescopes is challenging, and measurements are significantly altered due to the presence of the atmosphere. This should not be surprising, taking into account as we observe objects at farther distances, they are usually becoming more dimmer. Due to limitations of the instruments and atmospheric effects, objects will be hardly distinguishable from the background noise. Space based telescopes have a great advantage to ground based telescopes due to absence of atmospheric effects in measurements. Measurements

[4] http://www.ipac.caltech.edu/outreach/Edu/Windows/irwindows.html

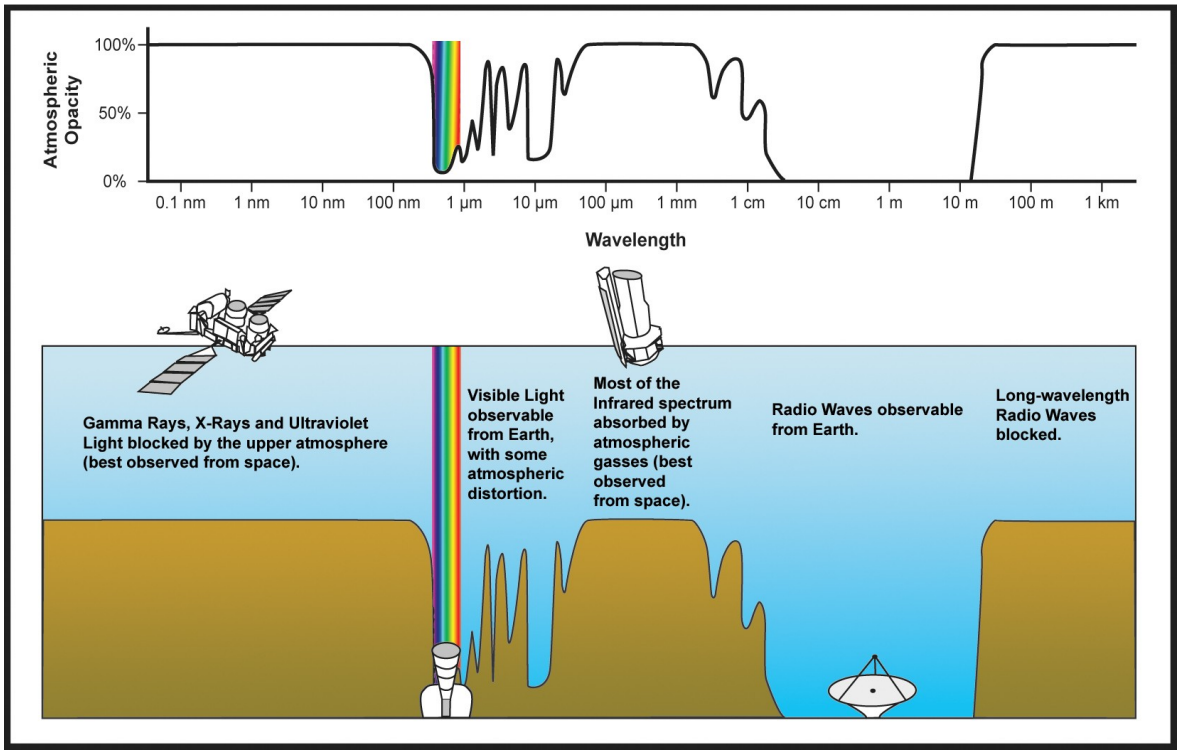

Figure 2.1: Opacity of the Earth's atmosphere to electromagnetic waves[4]

done by space based telescope are therefore more accurate, and the signal-to-noise ratio of a measurement performed by a ground based telescope is significantly lower compared to the signal-to-noise ratio of space based telescope, for the same integration time. Also, the spatial resolution of a space based telescopes is better by a factor of $\approx$ 5 - 10 compared to ground based telescopes.

It is a great advantage that the atmosphere is transparent to radio waves from about a couple of centimeters to about tens of meters. This means that radio waves in this wavelength range are not affected significantly by the atmosphere, and therefore reach us almost unaffected. Even though the atmosphere is transparent for radio waves in this wavelength range, a lot of calibrations and corrections need to be taken into account when observing in radio range. Signals from sources, especially extragalactic sources, are weak, so the noise in the signal needs to be removed. It is not possible to completely remove the noise, which comes from other sources on Earth, heating of the antennas, etc. Radio interferometers are almost ideal instruments on the Earth's surface for observing radio wavelengths from the source. Radio telescopes can be built as single dish telescopes, or as interferometers, an array of radio antennas, with configurations which can be arranged differently to achieve better resolution or better sensitivity of the source.

In the following subsections I will introduce the field in which sources analyzed in this work have been observed, and present the properties of instruments used for measuring the data used in this work.

2.1 COSMOS field

The Cosmic Evolution Survey (COSMOS) is a 2 square degree field on the sky, located in the region with little galactic extinction, so the observations of objects outside out galaxy can be performed without a contamination from our own galaxy. The goal of the COSMOS project is to study the formation and evolution of galaxies by examining their properties over a wide redshift range, and therefore observing galaxies at various cosmic times. Figure 2.2 shows the COSMOS field and its size compared to the size of the moon, and other surveys covered by the *Hubble Space Telescope*. The field itself is 16 times size of the moon. Many ground based and space based telescopes cover this field, giving the survey a multi-wavelength coverage. Covering the field with telescopes which observe at different wavelengths (X-ray, ultraviolet, optical, infrared, radio) is necessary because it provides the observer with information about properties of various components of galaxies such as interstellar medium, dust, stellar populations, and dark matter. Furthermore, ground-based spectroscopy at different wavelengths gives the information about redshift of sources, and the spectroscopic properties [24].

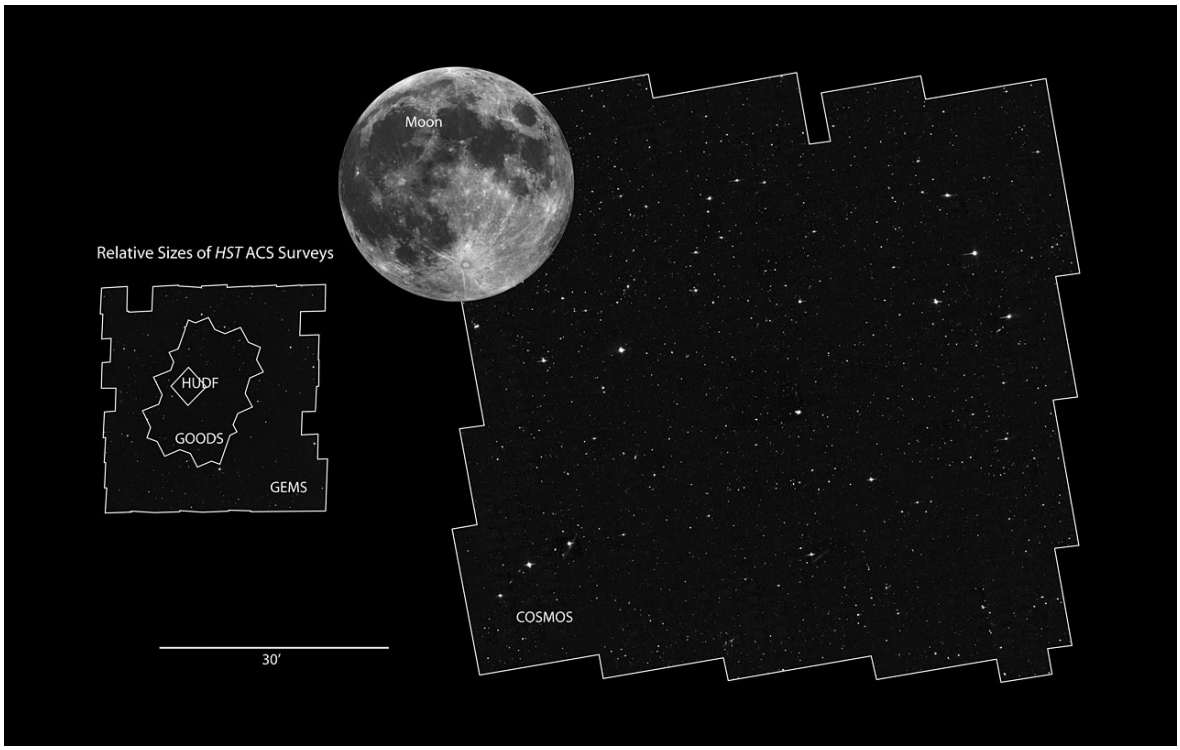

Figure 2.2: Size of the COSMOS field on the sky compared to the size of the full moon and relative sizes of HST based surveys[5]

2.2 HST WFC-3

The *Hubble Space Telescope* (HST) is one of world top instruments and crucial for the detailed study of galaxy formation in the optical and near-infrared wavelenghts. The latest installed camera on the HST - Wide Field Camera 3 (WFC-3) gives the ability to make very deep observations of galaxies at high redshift. Studying physical properties of high redshift galaxies using these high quality data provides us with a better insight and understanding of processes which drive the evolution of early type galaxies. The dataset used in this work has a high resolution measurements of 0.13”/pixel [6].

2.3 ALMA

The Atacama Large Millimeter Array (ALMA) probes the properties of galaxies in the sub-millimeter wavelengths, and at high redshift in the far-infrared wavelengths. ALMA is located in the Atacama desert, at the Chajnantor plateau. ALMA is specifically designed to probe rest-frame far-infrared emission of high redshift galaxies, and is capable of making sensitive measurements of dust and spectral lines, specifically [CII] emission line. Final version of the array will have 66 antennas, most of which will have dish of 12m in diameter, with adjustable configurations to distances from

[5] http://cosmos.astro.caltech.edu/page/public
[6] http://www.stsci.edu/hst/HST_overview


Figure 2.3: Left: The Hubble Space Telescope, image by NASA[8]; Right: The Atacama Large Millimeter Array, image by ESO[9]

150 meters to 16 kilometers [7]. Measurements used in this work were done using 20 antenna version of the array, and were conducted in cycle 1 in 2012.

Both instruments are shown in Figure 2.3 (left: the *Hubble Space Telescope*; right: the Atacama Large Millimeter Array)

2.4 Dataset

The original sample consists of 10 LBGs (9 normal galaxies and a quasar of low luminosity) [5] observed in the Cosmic Evolution Survey (COSMOS) field, which covers 2 square degrees on the sky. Galaxies in the sample along with their associated redshift are shown in Figure 2.4. After the optical examination of the images, I detected a companion close to one of the objects, thus I did the analysis for this additional object, making the total number of sources for the analysis 11. Objects in the sample are observed in the rest-frame far-infrared (FIR) by ALMA in cycle 1 (Principle Investigator: P. L. Capak) and in the rest-frame ultraviolet by the HST WFC-3 in cycle 22 (Principle Investigator: P. L. Capak).

This exact same sample of LBGs was analyzed by Capak et al. [5] using low signal-to-noise (S/N) ratio ground based data measured by the Ultra-VISTA Survey. Measurements by the HST WFC-3 were performed in three near-infrared (NIR) bands: F105W (1 μm), F125W (1.25 μm) and F160W (1.6 μm). Redshifts of objects in the sample are spectroscopically determined from the measurements done by the Deep Extragalactic Imaging Multi-Object Spectrograph (DEIMOS) which operates at optical wavelengths, and is installed at Keck II telescope at Mauna Kea, Hawaii. The HST WFC-3 high S/N ratio and high resolution ($\sim$ 0.13”/pixel) data enable us to accurately determine UV continuum slope values.

[7] http://www.almaobservatory.org/en/about-alma/how-does-alma-work/technology/interferometry

[8] http://spaceflight.nasa.gov/gallery/images/shuttle/sts-82/html/s82e5937.html

[9] http://www.eso.org/public/teles-instr/alma/

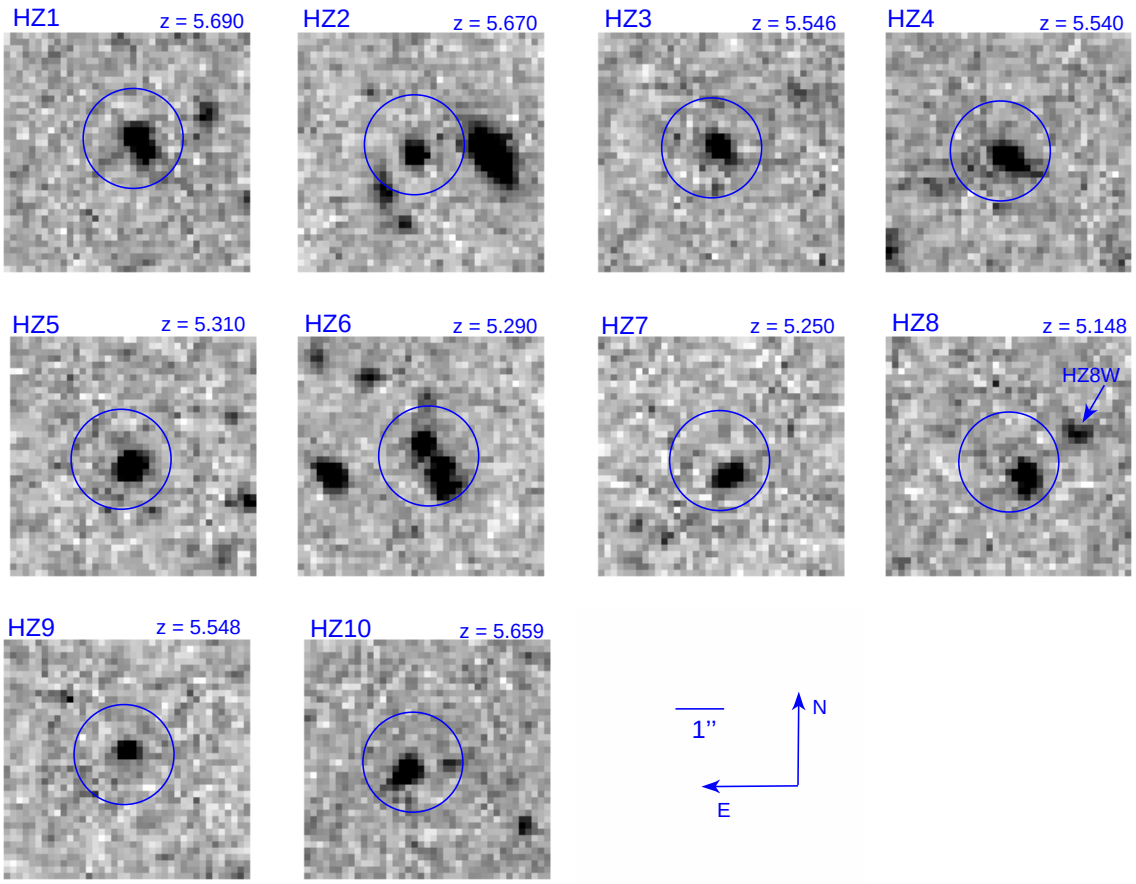

Figure 2.4: Cut-out images of sources from the sample in the F105W (1μm) band. Size of the cut-out images is 5”$\times$ 5” There are originally 9 galaxies and a quasar, however, the eighth object has a companion at a near redshift which I included as the additional source in the analysis. Images were taken by the Hubble Space Telescope Wide Field Camera 3 (HST WFC-3). Sources are in the center of each cut-out image, within the selected (blue circled) regions that have the radii of 1.02”. Sources in each cut-out image also contain their associated redshift.

3 MEASUREMENTS AND ANALYSIS

The UV continuum slope β is an indicator of the dust content in the line-of-sight of an observer. It is an important parameter, along with the infrared excess, that helps us to study and understand the properties of high redshift galaxies and how they compare to local galaxies. To be able to accurately determine UV continuum slope values, the flux density values need to be accurately measured from images. Accurately measuring flux density values can be challenging, due to the presence of the background noise which can significantly alter the measured flux density values. Simulations are therefore necessary to correct this effect, and to check for the uncertainties and possible biases of measured UV spectral slope β values. In this section I describe the method used to extract the flux density values from the sources in images, and different approaches I used to access uncertainties in computed β values.

For detection of sources in images and measurement of the photometry, I use the *Source Extractor* program. This program has many abilities, some of which are estimation of the background level, and detection of sources after setting the threshold level. By setting the threshold level, the program keeps all pixels with intensity above this threshold level and considers them as a signal, while pixels with intensity below this threshold level are treated as a background noise. Furthermore, the signal area is separated into objects, and properties of these objects are then being analyzed and written into catalogs [1]. The optimal threshold level chosen in this work to cut-off the background noise, while conserving the signal of sources was 2σ. This threshold level was determined by using *SAOImage DS9* to optically examine segmentation images generated by the *Source Extractor* program, used as well to extract the photometry of sources from images [1]. Except for setting the threshold level, choosing the aperture type also plays a significant role in extracting the photometry of detected objects.

The program supports three different aperture types which can be used to extract the photometry : ISO, AUTO, and manual aperture sizes. The ISO (isophotal) aperture forms the shape by following the pixels of constant brightness in the image. The AUTO (automatic) aperture is elliptically shaped and flexible to fit the size of the source in the image. The manual aperture is circularly shaped and its size can be manually chosen to fit the source. After optically examining the sources in images in the *SAOImage DS9*, I chose manual apertures to have radii of 0.77”, 0.9”, and 1.02”. These aperture radii were chosen so that the source fits within the aperture radius, without the contribution of the flux from surrounding sources. The extraction of photometry was performed on all objects in the sample using the same aperture size.

To extract the photometry I choose five different types of aperture : ISO, AUTO and three manually selected apertures. The *Source Extractor* generates a catalog which contains the photometry of all sources in the image. The photometry of sources in the sample was then found by cross-matching the known coordinates of sources

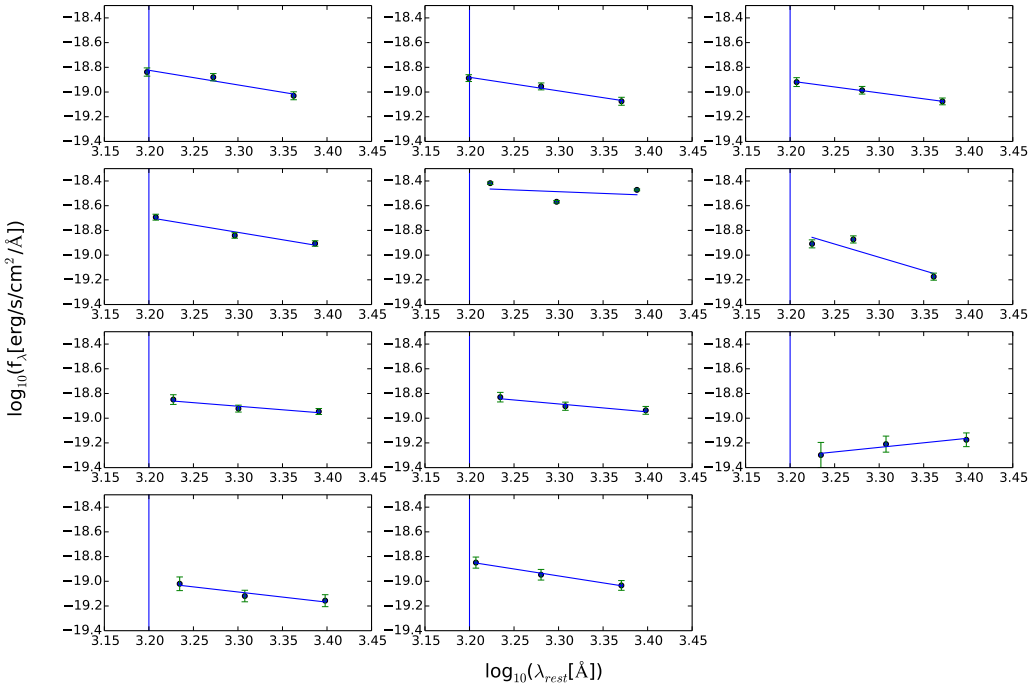

Figure 3.1: Logarithm of the flux density as a function of logarithm of the rest-frame wavelength λ_{rest} in each filter. Fitted slope to the points, in each panel, represents the UV continuum slope β, which is an indicator of the dust column density in galaxy. Blue vertical line represents the ultraviolet 1600 Å line.

with the coordinates of the sources in the catalog. The extracted photometry contains the flux density values of the sources of interest. Using the flux density values (order $\sim 10^{-19}$ [erg/sec/cm^2/Å]) I compute the value of the UV continuum slope β ($f_\lambda = \lambda_{rest}^{\beta}$). Figure 3.1 shows the observed flux density as a function of the rest-frame wavelength of the 11 sources in the log-log scale. The uncertainties of the flux density values are determined by the *Source Extractor* using the AUTO aperture to extract the photometry.

3.1 Accessing uncertainties in β measurements

The UV continuum slope β measurements depend on the flux density values extracted from images, and uncertainties in these flux measurements result directly in uncertainties in the UV continuum slope β measurements. In the following I outline the method used to determine the uncertainties and the accuracy on the measured β values by simulating mock galaxies.

3.1.1 Uncertainty of β from flux measurements

All of the observed flux density values of sources in the sample are taken as the mean flux density values for generating random Gaussian distributions. A single source has three different observed flux density values, measured in each band, and accordingly three random Gaussian distributions were generated per source. By varying the output flux values within each of the three randomly generated Gaussian distributions β values are found through 1000 iterations. Original β values computed from the flux density values extracted using the AUTO aperture, along with resultant median β values from Monte Carlo iterations are shown in Table 3.1. The uncertainty of the median β values were found as the 1σ of the Gaussian distribution of the output β values.

3.1.2 Simulating mock galaxies

To determine the systematic effects on computed β values and find the correction, I ran Monte Carlo simulations. Simulations are done using mock galaxies inserted at blank coordinates in images, i.e. that have no source detection in three bands, to find flux density values and accurately compute β value of the corresponding mock galaxy. Blank coordinates, i.e. empty pixels are found by stacking the segmentation images [10], generated by the *Source Extractor*, of a single source observed in three bands.

[10] Segmentation image is the image containing the patches attributed to objects detected in the original image [1]. The size of patches depends on the chosen aperture and the chosen threshold at which background noise is removed.

Table 3.1: The UV continuum slope β values computed from the original flux density values extracted photometrically using the AUTO aperture, and median β values obtained by varying flux density values within randomly generated Gaussian distributions.

Object name	β	median β
HZ1	-1.18	-1.19 $\pm$ 0.24
HZ2	-1.10	-1.10 $\pm$ 0.23
HZ3	-0.96	-0.96 $\pm$ 0.23
HZ4	-1.19	-1.20 $\pm$ 0.16
HZ5	-0.28	-0.28 $\pm$ 0.06
HZ6	-2.13	-2.14 $\pm$ 0.27
HZ7	-0.58	-0.58 $\pm$ 0.24
HZ8	-0.64	-0.64 $\pm$ 0.26
HZ8W	-0.74	0.74 $\pm$ 0.62
HZ9	-0.82	-0.83 $\pm$ 0.39
HZ10	-1.13	-1.13 $\pm$ 0.31

Mock galaxies, parametrized as 2D Gaussian, are generated and inserted into the original images at 100 randomly selected coordinates which correspond to empty pixels in the stacked segmentation image. The additional condition taken into account is that a square of 20x20 pixels around the randomly selected coordinate must be empty pixels as well. This way I am able to prevent the contamination of the signal of the mock source with fluxes from any nearby sources. As in the analysis for real galaxies, I use a detection and analysis threshold of 2σ.

Generated mock sources have ten fixed flux density values in a range [10^{-20}, 10^{-18}][erg/s/cm^2/Å] and each fixed flux density value has a 1000 randomly generated input β_{in} values in a range [-5,2]. The *Source Extractor* generates a catalog which contains the photometry of all sources found in the image. By cross-matching the known coordinates of mock sources with coordinates in output catalogs, I extract the photometry, so I can find the output β_{out} value using the output flux density values. Flux density value is related to the rest-frame wavelength at which the source is observed by f = λ_{rest}^{β} where f is the flux density, and λ_{rest} is the rest-frame wavelength. From this relation β value can be found from the best fit

$$\log_{10}(f) = \beta \cdot \log_{10}(\lambda_{rest}) + const. \tag{3.8}$$

if there are at least 2 flux density values of a mock source extracted from images by the *Source Extractor*. From the comparison of input β_{in} and output β_{out} values we can learn about systematic effects in measurements of output β_{out}, and determine the correction for β values that should be applied in the analysis of original sources.

3.1.3 Uncertainties of β using mock galaxies

After running the Monte Carlo simulations I compared the output β_{out} values to the input β_{in} values. The $\beta_{out} - \beta_{in}$ difference as a function of the nine fixed input AB magnitude values at 1600 Å is shown in Figure 3.2. This is a result of using the AUTO aperture to extract the photometry. The light blue dots represent the scatter of the difference between output and input β values. It is evident that the scatter is the largest in the case of the faintest fixed AB magnitude. When I insert a very faint mock galaxy in the original image (flux density values of the order of magnitude 10^{-20} [erg/s/cm^2/Å]) it can occur that it will not be detected by the *Source Extractor* in all three bands. Instead, it can be detected in two or only one band. In the case of a one - band detection the linear regression 3.8 can not be performed and β value can not be computed. If the galaxy is detected in two bands, the β value can be computed from the output flux density values, however, β values obtained this way are less precise when compared to the ones computed from detections which exist in all three bands, and the output β_{out} value differs significantly from the input β_{in} value (offset from 0 of the median value of difference in β is up to 25$\%$). Figure 3.2 shows median values (yellow circles) of the scatter of difference in β values, found from binning the x-axis to 5 intervals with equal number of scatter points. The horizontal dashed line represents the ideally expected value of the difference in the output and input β values, which is zero. The uncertainties of the $\beta_{out} - \beta_{in}$ for each fixed AB magnitude are defined as the 68th percentile of the distribution of the scatter. I find that all of the median values are consistent with zero within $< 5\%$. The results of Monte Carlo simulations based on mock galaxies show on average that systematic biases in β measurements for the galaxies in this sample are $\leq 2\%$. This is small compared to the measurement uncertainties of β that are $\leq 5\%$, and I therefore do not apply any correction.

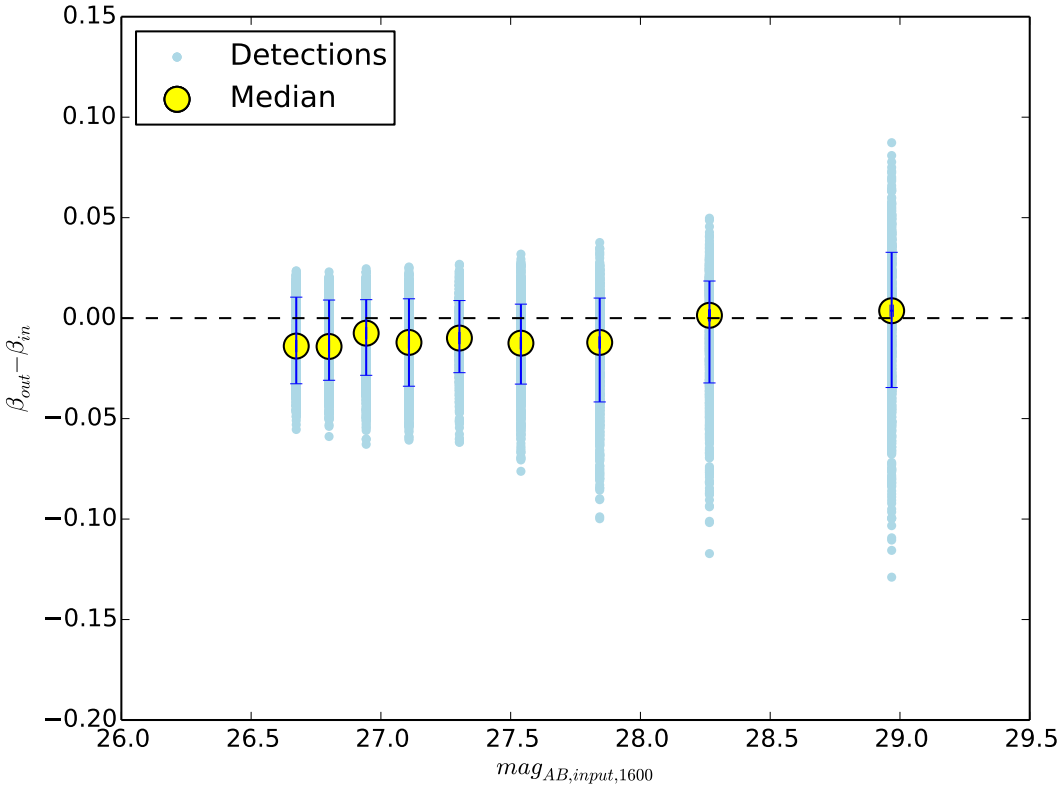

Figure 3.2: The difference between retrieved and input UV slope ($\beta_{out} - \beta_{in}$) as a function of the fixed input AB magnitude values at 1600 Å ($M_{AB,1600}$).

4 RESULTS

The UV continuum slope β from the spectral energy distribution fit is an estimate of the column density of the dust in galaxies. The infrared excess, i.e. the ratio of measured luminosities in the rest-frame infrared and ultraviolet part of the spectrum, is an estimate of the overall dust content in the galaxy. The properties of high redshift galaxies can be understood by comparing them to observed galaxies in the local universe. The relation between the infrared excess and the UV continuum slope β shows how the overall dust density and the dust content in the line-of-sight of an observer are linked in a galaxy, and thus helps us determine the amount of UV flux density re-radiated by dust in infrared [20]. Figure 4.1 shows the infrared excess as a function of the UV continuum slope (IRX vs. β) relation. The UV continuum slope values used in this plot are median output β values from Table 3.1 (see Section 3.1.1) obtained by using the AUTO aperture to extract the photometry.

In this work I tested for systematic bias in the measurements of β and the UV lumonosity using high S/N HST WFC-3 data. Blue filled and empty circles represent the results of this work based on the analysis of high S/N, high resolution HST WFC-3 data. The results of previous work, based on the low S/N ground based data from the UltraVISTA Survey [5] are represented by grey squares. The green solid curve shows the fit to the observed local star-burst systems that are rich with metal and dust content [20]. The green dashed curve represents the properties of the Small Magellanic Cloud (SMC) like system, which is characterized by its low metallicity and poor dust content [22, 17]. The results obtained by Capak et al. [5] showed that the dust content in systems at high redshift is lower compared to $z < 3$ galaxies confirming the predictions of previous studies that galaxies at higher redshift ($z > 3$) are bluer [3]. Continuum detections of the previous work were consistent with the Pettini dust curve, indicating that LBGs at $5 < z < 6$ are young systems with properties comparable to the SMC. The upper limits in their work were below the SMC curve indicating either systematic effects due to estimates of their β values, and UV or IR luminosities [5], e.g. possible overestimate of UV luminosities due to low S/N ratio ground based telescope data can result with low infrared excess values. The results of my work are mainly consistent with previous work [5], thus showing that systematic bias in measurements of β and UV luminosity can be ruled out and the differences between galaxies at high redshift and in the local universe are due to different physical properties present in high redshift ($z > 5$) systems.

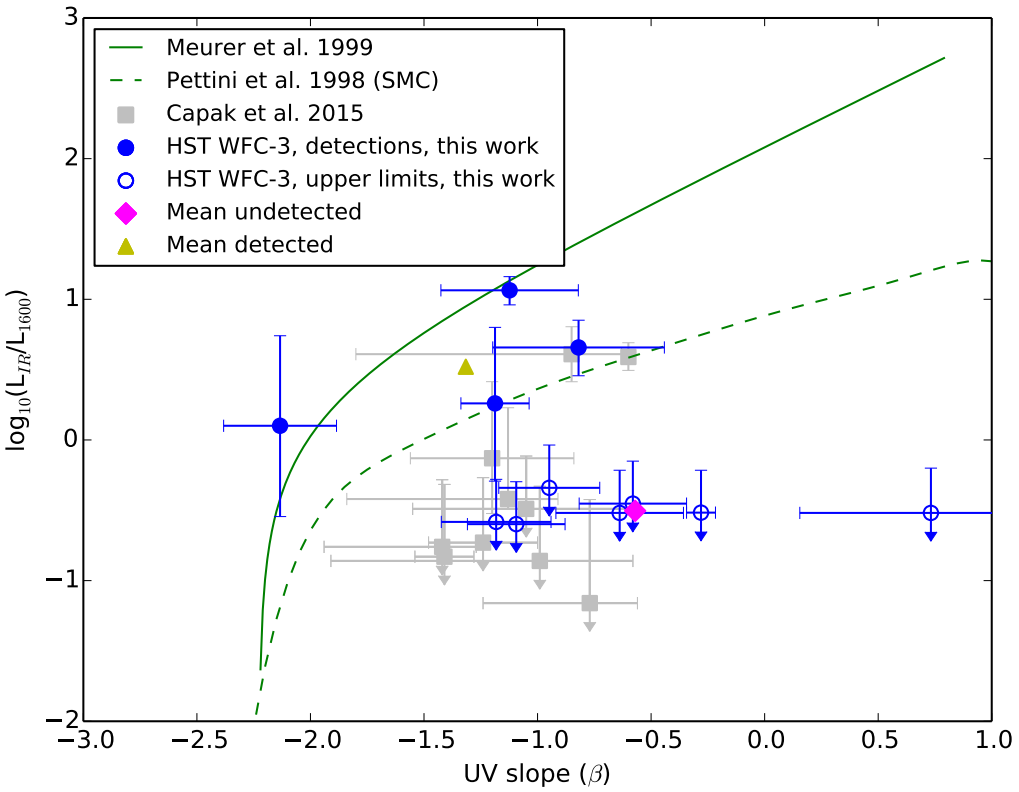

Figure 4.1: The infrared excess L_{IR}/L_{1600} as a function of the UV continuum slope β (IRX-β). Green solid curve is obtained by the fit to local star-burst systems found by Meurer et al. [20], while the green dashed curve represents the Pettini et al. [22] (SMC) like system. Blue circles (filled and empty) represent the results of this work. The subset of continuum detections (blue filled circles) is consistent with the Meurer-like curve, while the rest of the subset is consistent with the Pettini-like curve. The upper limit detections are below the Pettini-like curve. Results of this work are consistent with the previous work (grey squares, [5]).

5 DISCUSSION

This work shows consistency with results of previous work by Capak et al. [5]. The UV luminosity values (L_{1600}) obtained from the HST WFC-3 measurements are lower by 28% on average, compared to estimated UV luminosity values from measurements by the ground based telescope, therefore resulting in higher IRX value. The IRX value is an estimate of the total amount of dust in the galaxy. Therefore, higher IRX values indicate that galaxies in the sample contain more dust then previously shown. The mean β value for galaxies detected in the dust continuum in this work is $\langle\beta\rangle \sim$ -1.3 compared to $\langle\beta\rangle \sim$ - 0.9 of the previous work, while the mean β value for galaxies undetected in the dust continuum is $\langle\beta\rangle \sim$ - 0.6, compared to the mean value of undetected in the previous work $\langle\beta\rangle \sim$ -1.2. A subset of continuum detections in this work (blue filled circles) shows consistency with the Meurer-like curve, indicating that these systems are possibly already evolved, seemingly similar in their properties to local star-burst galaxies, rich in metal and dust content. The rest of the continuum subset is consistent with the Pettini-like curve, indicating that these systems possibly show properties similar to local young systems with low dust content, similar to the SMC. However, the upper limit detections are below the Pettini-like curve, indicating a different dust geometry, possibly its higher temperature, and different gas dynamics at high redshift galaxies (z $>$ 5) compared to galaxies in the local universe. The results of this work indicate that our sample consists of two populations of galaxies. Roughly, one population of metal-rich and dust-rich systems, therefore similar with their properties to local star-burst galaxies, and the other population of young, un-evolved, dust-poor and metal-poor systems with similar properties to the SMC. Furthermore, the possible existence of two distinct populations of galaxies approximately 1 Gyr after the Big Bang might therefore indicate a rapid evolution of galaxies in the time following the epoch of re-ionization.

I examine the spectra of galaxies in the sample to determine which of them are Lyman-alpha (Ly-α) emitters, or weak/no Ly-α emitters. Figure 5.1 shows the IRX vs. β relation, with blue squares representing galaxies in the sample that are strong Ly-α emitters, red circle represents the galaxy with weak Ly-α emission, and black triangle represents a galaxy with no detected Ly-α emission in the spectrum. These results are partly consistent with the analysis done by Faisst et al. [11] which shows that weak/no Ly-α emission may originate in dust-rich and metal-rich galaxies, similar in their properties to local star-burst systems, while strong Ly-α emission may be attributed to dust-poor and metal-poor galaxies with young stellar populations, comparable in their properties to the SMC. Still, more LBGs at various redshifts need to be observed to cover a wide population of galaxies with different physical properties in order to make qualitative conclusions in terms of the existence of a correlation between Ly-α emission from galaxies and their position in the IRX - β plot.

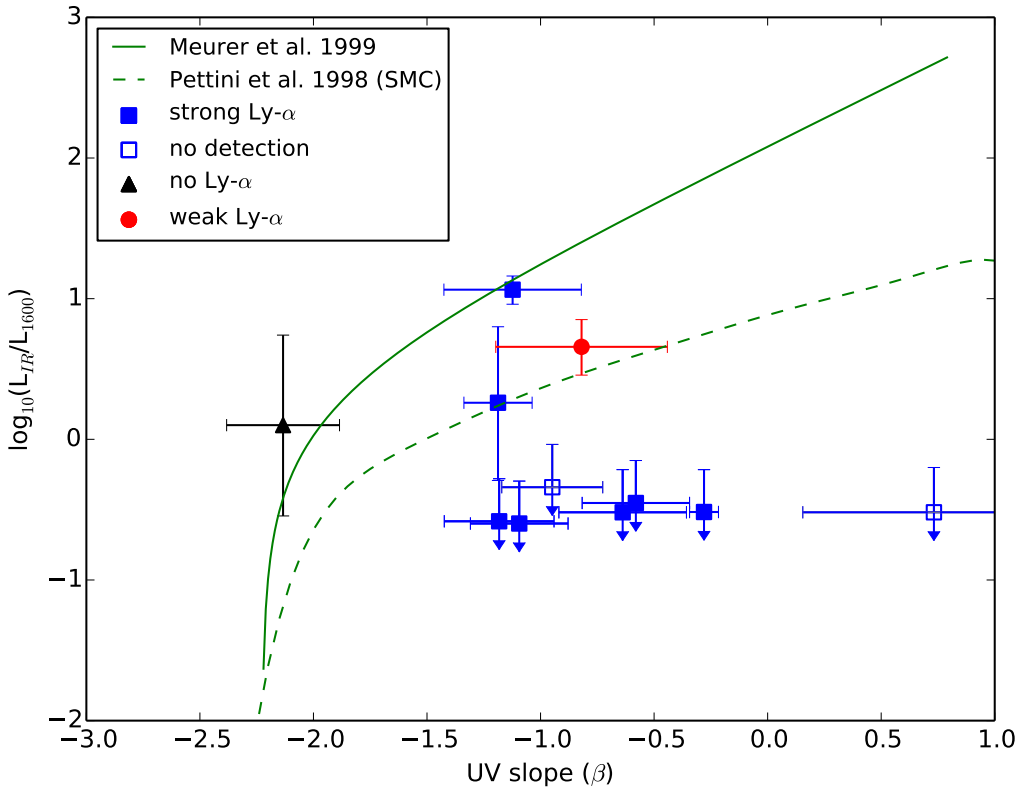

Figure 5.1: The IRX-β relation, combined with Ly-α candidates among sources in the sample. Blue squares represent sources in the sample which are observed to be strong Ly-α emitting galaxies. More observations are needed at this and other redshifts to make conclusions about the correlation between Ly-α emitting galaxies and their position in the IRX-β plot.

6 CONCLUSION

In this work I studied dust properties of 11 LBGs at a redshift range $5 < z < 6$, which in terms of the age of the universe corresponds to 1 billion years after the Big Bang. I used deep high resolution and high sensitivity measurements obtained by the HST WFC-3 in NIR in 3 bands to find the dust column density, otherwise known as the UV spectral slope β, of galaxies in the sample and to compute the luminosity of galaxies in the rest-frame UV. Known rest-frame FIR measurements of luminosities obtained by ALMA were used along with rest-frame UV luminosities to find the infrared excess, which is defined as the ratio of FIR to UV luminosity. From comparing the results of this work to the previous results [5], the main conclusions of this work are following

- I find the mean β value for galaxies undetected in dust continuum of $\langle\beta\rangle \sim$ - 0.6, compared to the mean value of $\langle\beta\rangle \sim$ - 1.2 in the previous work [5]. Also, the mean value of β for galaxies detected in dust continuum is $\langle\beta\rangle \sim$ - 1.3, while the mean in the previous work is $\langle\beta\rangle \sim$ - 0.9.

- A subset of continuum detections is seemingly consistent with the Meurer - like curve, the fit to local star-burst galaxies, while the other part of the subset is consistent with the Pettini - like curve, i.e. SMC like system. Upper limits are still being below the Pettini - like curve, showing consistency with previous work.

- The results of this work are indicative of the existence of possibly two distinct populations of galaxies at $5 < z < 6$, one of which are evolved, metal-rich and dust-rich systems, and the second population of young, metal-poor and dust-poor systems.

- The results are in good agreement with the findings of Faisst et al. [11], which show that Ly-α emitting galaxies may be similar in their properties to local dust-poor and metal-poor systems, while weak/no Ly-α emission may be present in galaxies similar in their properties to local star-burst galaxies. However, more data is needed to be able to draw conclusions about the connection between Ly-α emission from galaxies and their position in the IRX - β plot.

6.1 Outlook

As mentioned previously, to measure the SFR of galaxies, one can either find a correction for the dust extinction, or measure separately the UV and IR SFR. Finding the correction for the effect of the absorption by dust is not an easy task and requires modeling of galaxies with different star-formation histories, dust abundance, age, etc. Kong et al. [16] found the relation for the absorption coefficient in local galaxies

$$A_{FUV} = \frac{(A_0 + A_1)(x - x_0)}{2} + \frac{A_1 - A_0)\sigma_0}{2} \ln\left[\cosh\left(\frac{x - x_0}{\sigma_0}\right)\right] + A_2 \tag{6.9}$$

They found the relation from the fit of the A_{FUV} in terms of the IRX and β values from the library of galaxy models they developed. The main advantage of this relation is that it depends on the IRX parameter (x) and not on β, since the IRX is independent on the dust geometry within the galaxy and hence a better estimator of the absorption coefficient. In the case when infrared luminosity is not available, the absorption coefficient for local galaxies can be estimated from the following relation they found, which relies on the β value

$$A_{FUV} = 3.87 + 1.87\,(\beta_{GLX} + 0.4 \log b) \tag{6.10}$$

though this relation may result in higher uncertainty in the estimated absorption coefficient since β depends on the dust geometry.

Nevertheless, it is not sure whether these relations hold for galaxies at higher redshifts (z $>$ 4) as they may exhibit different dust properties in terms of dust geometry and gas dynamics compared to galaxies at lower redshifts. The additional reason is that the star-formation rate density changes through cosmic time, having a peak around z = 2, and declining afterwards, while up to z = 2 it is raising. To check whether the relations above hold for this sample of galaxies, I will develop a separate model of galaxies assuming a wide range of star-formation histories, dust content, age of galaxies, etc. to quantify the absorption coefficient which will lead to understanding to which extent the UV rest-frame emission is being attenuated by dust.

REFERENCES

[1] Bertin, E. and Arnouts, S. (1996). SExtractor: Software for source extraction. *Astronomy and Astrophysics, Supplement*, 117:393–404.

[2] Boquien, M., Buat, V., Boselli, A., Baes, M., Bendo, G. J., Ciesla, L., Cooray, A., Cortese, L., Eales, S., Gavazzi, G., Gomez, H. L., Lebouteiller, V., Pappalardo, C., Pohlen, M., Smith, M. W. L., and Spinoglio, L. (2012). The IRX-β relation on subgalactic scales in star-forming galaxies of the Herschel Reference Survey. *Astronomy and Astrophysics*, 539:A145.

[3] Bouwens, R. J., Illingworth, G. D., Oesch, P. A., Franx, M., Labbé, I., Trenti, M., van Dokkum, P., Carollo, C. M., González, V., Smit, R., and Magee, D. (2012). UV-continuum Slopes at z ˜ 4-7 from the HUDF09+ERS+CANDELS Observations: Discovery of a Well-defined UV Color-Magnitude Relationship for z >= 4 Star-forming Galaxies. *The Astrophysical Journal*, 754:83.

[4] Bruzual, G. and Charlot, S. (2003). Stellar population synthesis at the resolution of 2003. *Monthly Notices of the Royal Astronomical Society*, 344:1000–1028.

[5] Capak, P. L., Carilli, C., Jones, G., Casey, C. M., Riechers, D., Sheth, K., Carollo, C. M., Ilbert, O., Karim, A., Lefevre, O., Lilly, S., Scoville, N., Smolcic, V., and Yan, L. (2015). Galaxies at redshifts 5 to 6 with systematically low dust content and high [C II] emission. *Nature*, 522:455–458.

[6] Charlot, S. and Fall, S. M. (2000). A Simple Model for the Absorption of Starlight by Dust in Galaxies. *The Astrophysical Journal*, 539:718–731.

[7] da Cunha, E., Charlot, S., and Elbaz, D. (2008). A simple model to interpret the ultraviolet, optical and infrared emission from galaxies. *Monthly Notices of the Royal Astronomical Society*, 388:1595–1617.

[8] Daddi, E., Dickinson, M., Morrison, G., Chary, R., Cimatti, A., Elbaz, D., Frayer, D., Renzini, A., Pope, A., Alexander, D. M., Bauer, F. E., Giavalisco, M., Huynh, M., Kurk, J., and Mignoli, M. (2007). Multiwavelength Study of Massive Galaxies at z˜2. I. Star Formation and Galaxy Growth. *The Astrophysical Journal*, 670:156–172.

[9] Draine, B. T. and Li, A. (2001). Infrared Emission from Interstellar Dust. I. Stochastic Heating of Small Grains. *The Astrophysical Journal*, 551:807–824.

[10] Elbaz, D., Daddi, E., Le Borgne, D., Dickinson, M., Alexander, D. M., Chary, R.-R., Starck, J.-L., Brandt, W. N., Kitzbichler, M., MacDonald, E., Nonino, M., Popesso, P., Stern, D., and Vanzella, E. (2007). The reversal of the star formation-density relation in the distant universe. *Astronomy and Astrophysics*, 468:33–48.

[11] Faisst, A. L., Capak, P. L., Davidzon, I., Salvato, M., Laigle, C., Ilbert, O., Onodera, M., Hasinger, G., Kakazu, Y., Masters, D., Mobasher, B., Sanders, D., Silverman, J. D., Yan, L., and Scoville, N. Z. (2015). Rest-UV Absorption Lines as Metallicity Estimator: the Metal Content of Star-Forming Galaxies at z˜5. *ArXiv e-prints*.

[12] Galametz, M., Kennicutt, R. C., Albrecht, M., Aniano, G., Armus, L., Bertoldi, F., Calzetti, D., Crocker, A. F., Croxall, K. V., Dale, D. A., Donovan Meyer, J., Draine, B. T., Engelbracht, C. W., Hinz, J. L., Roussel, H., Skibba, R. A., Tabatabaei, F. S., Walter, F., Weiss, A., Wilson, C. D., and Wolfire, M. G. (2012). Mapping the cold dust temperatures and masses of nearby KINGFISH galaxies with Herschel. *Monthly Notices of the Royal Astronomical Society*, 425:763–787.

[13] Giavalisco, M. (2002). Lyman-Break Galaxies. *Annual Review of Astronomy and Astrophysics*, 40:579–641.

[14] Hayes, M. (2015). Lyman Alpha Emitting Galaxies in the Nearby Universe. *Publications of the Astronomical Society of Australia*, 32:e027.

[15] Hu, E. M., Cowie, L. L., and McMahon, R. G. (1998). The Density of Lyα Emitters at Very High Redshift. *The Astrophysical Journal Letters*, 502:L99–L103.

[16] Kong, X., Charlot, S., Brinchmann, J., and Fall, S. M. (2004). Star formation history and dust content of galaxies drawn from ultraviolet surveys. *Monthly Notices of the Royal Astronomical Society*, 349:769–778.

[17] Li, A. and Draine, B. T. (2002). Infrared Emission from Interstellar Dust. III. The Small Magellanic Cloud. *The Astrophysical Journal*, 576:762–772.

[18] Madau, P. and Dickinson, M. (2014). Cosmic Star-Formation History. *Annual Review of Astronomy and Astrophysics*, 52:415–486.

[19] Madau, P., Pozzetti, L., and Dickinson, M. (1998). The Star Formation History of Field Galaxies. *The Astrophysical Journal*, 498:106–116.

[20] Meurer, G. R., Heckman, T. M., and Calzetti, D. (1999). Dust Absorption and the Ultraviolet Luminosity Density at z ˜ 3 as Calibrated by Local Starburst Galaxies. *The Astrophysical Journal*, 521:64–80.

[21] Noeske, K. G., Weiner, B. J., Faber, S. M., Papovich, C., Koo, D. C., Somerville, R. S., Bundy, K., Conselice, C. J., Newman, J. A., Schiminovich, D., Le Floc'h, E., Coil, A. L., Rieke, G. H., Lotz, J. M., Primack, J. R., Barmby, P., Cooper, M. C., Davis, M., Ellis, R. S., Fazio, G. G., Guhathakurta, P., Huang, J., Kassin, S. A., Martin, D. C., Phillips, A. C., Rich, R. M., Small, T. A., Willmer, C. N. A., and Wilson, G. (2007). Star Formation in AEGIS Field Galaxies since z=1.1: The

Dominance of Gradually Declining Star Formation, and the Main Sequence of Star-forming Galaxies. *The Astrophysical Journal Letters*, 660:L43–L46.

[22] Pettini, M., Kellogg, M., Steidel, C. C., Dickinson, M., Adelberger, K. L., and Giavalisco, M. (1998). Infrared Observations of Nebular Emission Lines from Galaxies at Z ˜ = 3. *The Astrophysical Journal*, 508:539–550.

[23] Purcell, E. M. (1976). Temperature fluctuations in very small interstellar grains. *The Astrophysical Journal*, 206:685–690.

[24] Scoville, N. (2007). The Cosmic Evolution Survey: COSMOS. In Baker, A. J., Glenn, J., Harris, A. I., Mangum, J. G., and Yun, M. S., editors, *From Z-Machines to ALMA: (Sub)Millimeter Spectroscopy of Galaxies*, volume 375 of *Astronomical Society of the Pacific Conference Series*, page 166.

[25] Smith, J. D. T., Draine, B. T., Dale, D. A., Moustakas, J., Kennicutt, Jr., R. C., Helou, G., Armus, L., Roussel, H., Sheth, K., Bendo, G. J., Buckalew, B. A., Calzetti, D., Engelbracht, C. W., Gordon, K. D., Hollenbach, D. J., Li, A., Malhotra, S., Murphy, E. J., and Walter, F. (2007). The Mid-Infrared Spectrum of Star-forming Galaxies: Global Properties of Polycyclic Aromatic Hydrocarbon Emission. *The Astrophysical Journal*, 656:770–791.

[26] Speagle, J. S., Steinhardt, C. L., Capak, P. L., and Silverman, J. D. (2014). A Highly Consistent Framework for the Evolution of the Star-Forming "Main Sequence" from z ˜ 0-6. *The Astrophysical Journal Supplement Series*, 214:15.

[27] Steidel, C. C., Pettini, M., and Adelberger, K. L. (2001). Lyman-Continuum Emission from Galaxies at Z ˜ = 3.4. *The Astrophysical Journal*, 546:665–671.

[28] Toft, S., van Dokkum, P., Franx, M., Labbe, I., Förster Schreiber, N. M., Wuyts, S., Webb, T., Rudnick, G., Zirm, A., Kriek, M., van der Werf, P., Blakeslee, J. P., Illingworth, G., Rix, H.-W., Papovich, C., and Moorwood, A. (2007). Hubble Space Telescope and Spitzer Imaging of Red and Blue Galaxies at z ˜ 2.5: A Correlation between Size and Star Formation Activity from Compact Quiescent Galaxies to Extended Star-forming Galaxies. *The Astrophysical Journal*, 671:285–302.

[29] Weingartner, J. C. and Draine, B. T. (2001). Dust Grain-Size Distributions and Extinction in the Milky Way, Large Magellanic Cloud, and Small Magellanic Cloud. *The Astrophysical Journal*, 548:296–309.

Appendices

Appendix A

Figure A.1 shows the difference between the output and input UV continuum slope values as a function of the output AB magnitude at 1600 Å. This plot is the result of using the AUTO aperture in extracting the photometry of the sources by the *Source Extractor*. For the comparison, the resultant plot of using the manual aperture of radius 0.9" to extract the photometry is shown in Figure A.2. These plots contain ten panels, each panel for a fixed input AB magnitude value at 1600 Å indicated on the top of the associated panel. The x-axis which plots the output AB magnitude at 1600 Å in each panel has been divided into five intervals so that each interval contains equal number of $\beta_{out} - \beta_{in}$ values. For each interval I find the median value of the scattered $\beta_{out} - \beta_{in}$ distribution (yellow circles). The uncertainties of both x and y-axis are found as the 68th percentile of the distribution of output AB magnitudes at 1600 Å and $\beta_{out} - \beta_{in}$ values. It is evident from Figure A.1 that median values are systematically inconsistent with the expected value of zero for fainter magnitudes. The median values of $\beta_{out} - \beta_{in}$ are more consistent with the expected value in the case when the manual aperture is chosen for the photometry. The offset is less then 2%, and this correction does not change the output values of β significantly. The additional reason for this inconsistency could be due to the chosen wide input β value range of [-5,2].

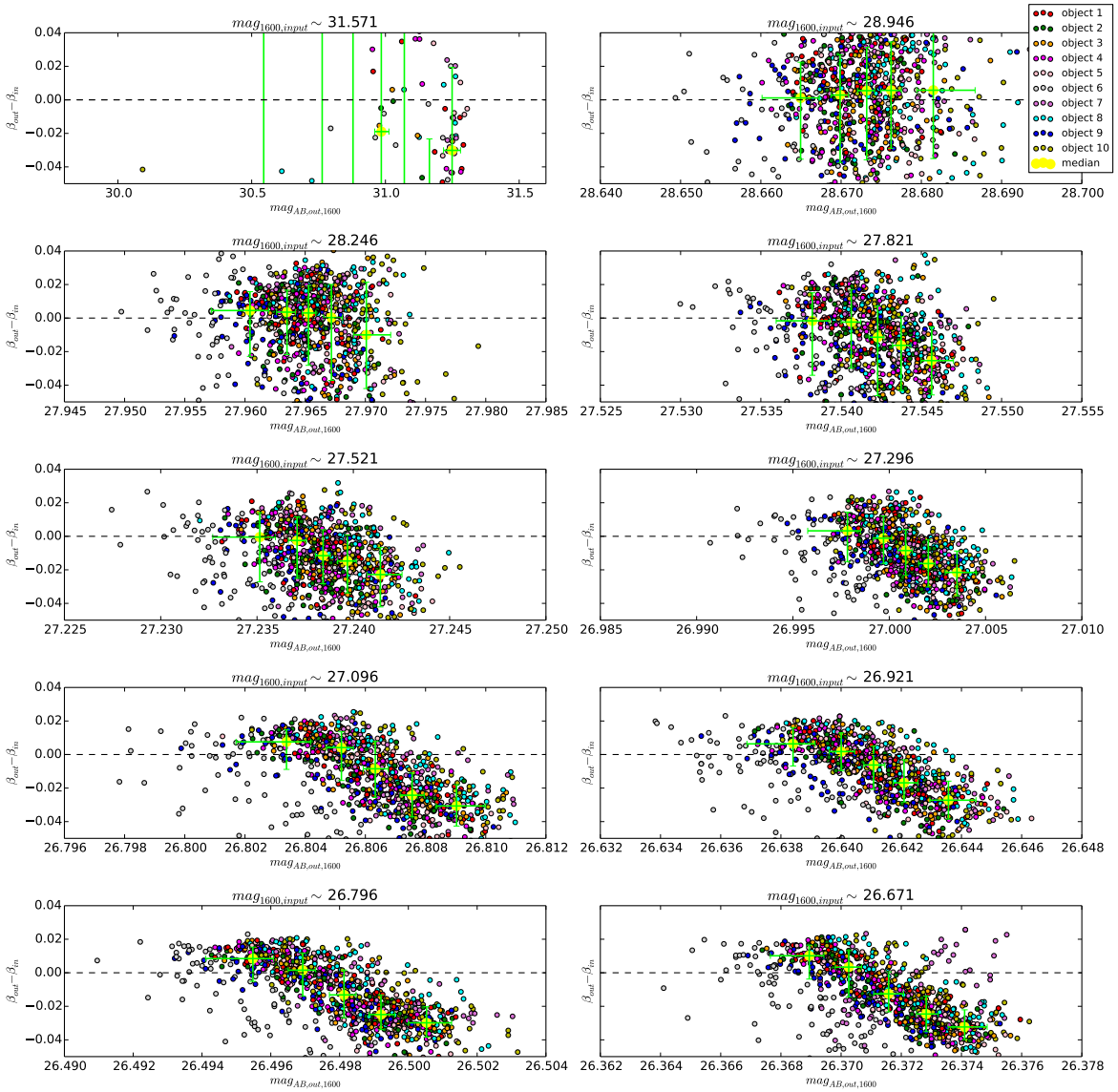

Figure A.1: The difference in continuum UV slope values ($\beta_{out} - \beta_{in}$) as a function of the output AB magnitude values at 1600 Å. On top of each panel is the value of the fixed input AB magnitude at 1600 Å. The AUTO (elliptically shaped) aperture was selected to extract the photometry of the sources. The interval on the x-axis is divided in each panel into 5 intervals so that each interval contains the exact same number of ($\beta_{out} - \beta_{in}$) values. Yellow circles represent the median values of the ($\beta_{out} - \beta_{in}$) scatter in each interval. The uncertainties on both axes are found as the 68th percentile of the scattered distribution. There is a systematic offset in median values for brighter magnitudes towards bluer values of the difference in UV continuum slope measurements, which indicates systematically bluer output β_{out} values for sources brighter than 27 AB magnitude.

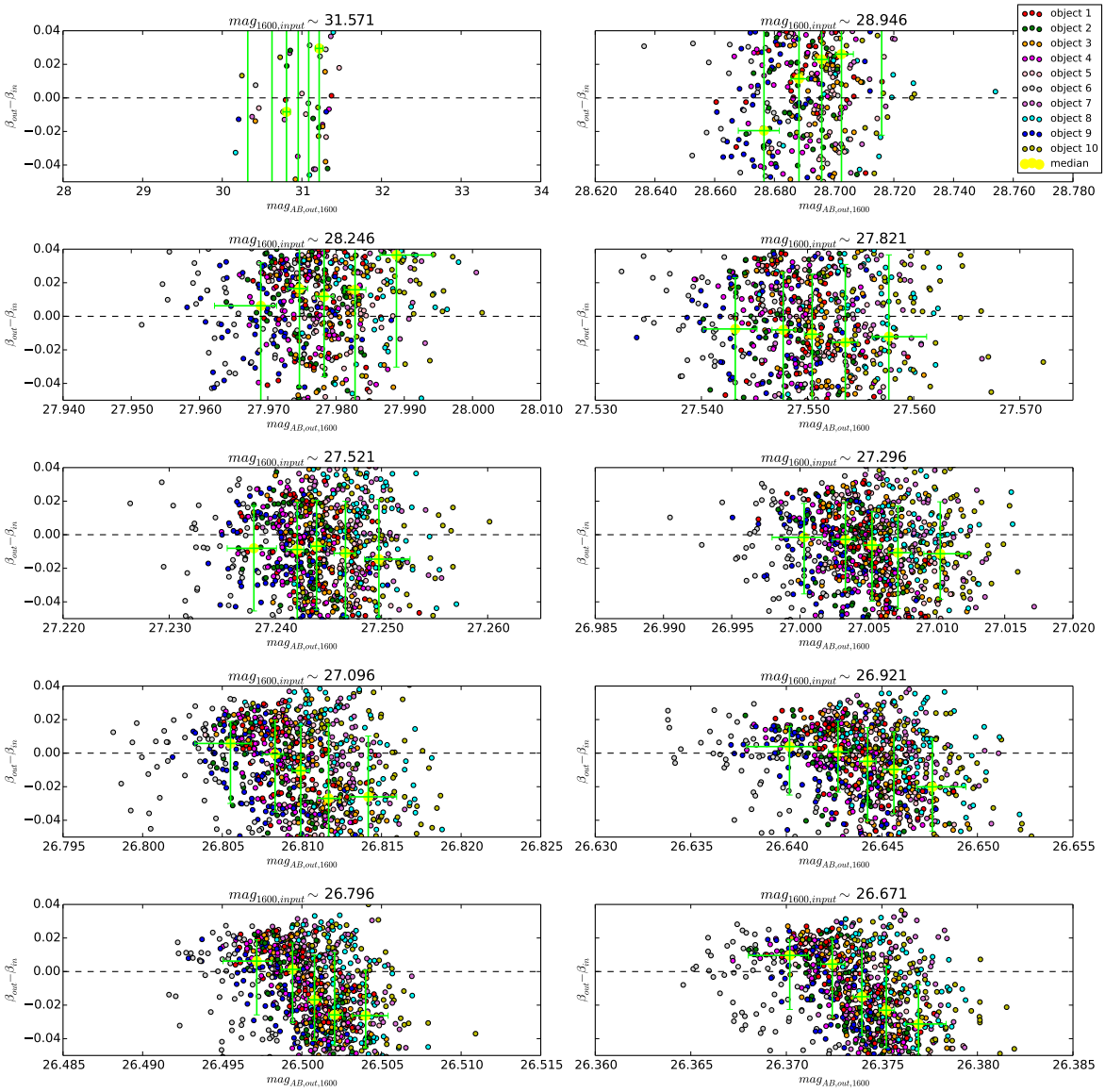

Figure A.2: The difference in continuum UV slope values ($\beta_{out} - \beta_{in}$) as a function of the output AB magnitude values at 1600 Å. On top of each panel is the value of the fixed input AB magnitude at 1600 Å. This is the result of using manual aperture (circularly shaped) to extract the photometry. The radius of the manual aperture is 0.9". Yellow circles represent median values of each sub-interval on the x axis. The uncertainties on both axes are found as the 68th percentile of the scattered distribution. The systematic offset is also present in the case when manual aperture is chosen for the photometry.

7 Prošireni sažetak (Extended abstract)

Proučavanje svojstava galaksija na visokim crvenim pomacima vodi nas k boljem razumijevanju formiranja i evolucije galaksija kroz kozmičko vrijeme. U ovom radu proučavam svojstva galaksija na crvenom pomaku $5 < z < 6$ kako bih istražila njihove metalicitete i stupanj formiranja novih zvijezda (eng. *star-formation rate*). Navedeni crveni pomak odgovara otprilike 1 milijardu godina starom svemiru, nakon Velikog Praska.

Prisutnost prašine u međuzvjezdanom mediju u galaksijama vrlo često djelomično blokira ultraljubičasto zračenje mladih i vrućih zvijezda u galaksijama. S obzirom da će fotoni mladih zvijezda ultraljubičastih valnih duljina biti raspršeni i apsorbirani na prašini, ona onemogućava mjerenje stupnja formiranja novih zvijezda samo na temelju opažanja galaksija u ultraljubičastom dijelu spektra u sustavu mirovanja galaksija. No, nakon apsorpcije fotona ultraljubičastih valnih duljina na prašini, prašina će se zagrijati te će emitirati zračenje u infracrvenim valnim duljinama. Smatra se kako fotoni infracrvenih valnih duljina neće dalje biti apsorbirani na prašini u međuzvjezdanom mediju, stoga se mjerenjem emisije iz galaksije u infracrvenom dijelu spektra može mjeriti stvaranje novih zvijezda u infracrvenom. Ukupan stupanj formiranja novih zvijezda tada se može pronaći zbrajanjem stupnja formiranja novih zvijezda u infracrvenom i ultraljubičastom dijelu spektra. Na visokim crvenim pomacima emisija iz galaksija u infracrvenom dijelu spektra u sustavu mirovanja galaksija teško se može mjeriti s obzirom na trenutna ograničenja instrumenata. Kako bi se onda mogla procijeniti ekstinkcija na prašini koriste se mjerenja količine prašine u smjeru doglednice promatrača (β) koja se dobivaju uz pomoć flukseva mjerenih u ultraljubičastom dijelu spektra u sustavu mirovanja galaksija. Iz izmjerenog fluksa u ultraljubičastom dijelu spektra također se može naći i odgovarajući luminozitet u ultraljubičastom, pa je omjer luminoziteta u infracrvenom i ultraljubičastom (eng. *infrared excess*, IRX) onda pokazatelj ukupne količine prašine u galaksiji. Korelacija između tih dviju veličina (IRX - β) daje informaciju o ukupnoj količini zračenja u ultraljubičastom dijelu spektra izračenim iz prašine u infracrvenom dijelu spektra.

Uzorak galaksija koji analiziram čini 10 galaksija, od kojih je 9 galaksija normalnog tipa koje su aktivne u formiranju novih zvijezda, te jedan kvazar. Galaksije u uzorku su tzv. (eng) *Lyman break* galaksije. Taj tip galaksija je poseban po tome što u spektru imaju karakterističan diskontinuitet na valnoj duljini 912 Å . Taj diskontinutitet u spektru posljedica je apsorpcije fotona valne duljine kraće od 912 Å u plinu i prašini. Ovisno o optičkoj dubini medija na koji naiđu takvi visoko energetski fotoni, samo će rijetki biti raspršeni van galaksije. Zbog tog razloga se galaksije čine blijeđe za valne duljine kraće od valne duljine diskontinuiteta. Prilikom optičke analize galaksija uočila sam da jedna od normalnih galaksija na slici ima galaksiju pratioca na vrlo bliskom crvenom pomaku. Uključivanjem dodatne galaksije u analizu, konačan uzorak za koji sam provela analizu sadrži ukupno jedanaest galaksija.

Galaksije u uzorku su opažene sa svemirskim teleskopom *Hubble Space Telescope* Wide Field Camera 3 u bliskom infracrvenom dijelu spektra sa 3 filtera. S obzirom na crveni pomak galaksija u uzorku, opažanje u bliskim infracrvenim valnim duljinama odgovara emisiji u ultraljubičastom dijelu spektra u sustavu mirovanja galaksija. Opažanje emisije iz galaksija u ultraljubičastom dijelu spektra nam daje informaciju o stupnju formiranja novih zvijezda. Nadalje, pomoću informacije o emisiji iz galaksije u uljtraljubičastom dijelu spektra može se odrediti koliki je luminozitet galaksije u tom dijelu spektra. Osim luminoziteta, opažanja u ultraljubičastom dijelu spektra u 3 filtera mogu poslužiti kao indikator količine prašine u smjeru doglednice promatrača.

Galaksije su još bile opažene sa zemaljskim teleskopom Atacama Large Millimeter Array. Taj teleskop je set radio interferometara koji su u ovom slučaju opažali zračenje iz galaksija u dalekim infracrvenim valnim duljinama u sustavu mirovanja galaksija. Opažanja u dalekim infracrvenim valnim duljinama u sustavu mirovanja galaksija su pokazatelj distribucije prašine i [CII] plina u opaženim galaksijama, pa je pomoću tih opažanja moguće doći do luminoziteta galaksija u dalekom infracrvenom dijelu spektra. Omjer luminoziteta galaksija u daleko infracrvenim i ultraljubičastim valnim duljinama govori nam kolika je ukupna količina prašine u čitavoj galaksiji. Taj je parametar neovisan o geometriji prašine u galaksijama i kao takav je vrlo dobar pokazatelj ukupne količine prašine u galaksiji. Nadalje, parametar koji opisuje količinu prašine u smjeru doglednice promatrača (eng. *line-of-sight*) zove se ultraljubičasti spektralni nagib (eng. *ultraviolet spectral slope*, β). Taj je parametar jako ovisan o geometriji prašine, te također ovisi o samim svojstvima prašine.

S obzirom da je emitirana energija iz galaksija u uzorku mjerena sa *Hubble Space Telescope* Wide Field Camera 3 u tri filtera u bliskom infracrvenom dijelu spektra (F105 - 1μm, F125 - 1.25μm, F160 - 1.6μm) imam na raspolaganju 3 vrijednosti fluksa. Fluks je količina energije koju promatrač primi po jedinici površine u jedinici vremena. Iz relacije koja povezuje fluks i valnu duljinu, moguće je izračunati parametar koji opisuje količinu prašine u galaksiji u smjeru doglednice promatrača pomoću linearne regresije. Nadalje, kako na raspolaganju imam omjer luminoziteta u ultraljubičastom dijelu spektra i luminozitet u infracrvenom dijelu spektra, te vrijednost ultraljubičastog spektralnog nagiba, mogu provjeriti kako omjer luminoziteta ovisi o ultraljubičastom spektralnom nagibu.

Prijašnji rad [5] koristi isti uzorak galaksija koji je analiziran i u ovom radu, no za razliku od opažanja u ovom radu, za dobivanje luminoziteta u ultraljubičastom dijelu spektra koristili su podatke sa zemaljskih teleskopa UltraVISTA Survey. Za luminozitete u infracrvenom dijelu spektra također su koristili opažanja sa radio interferometara Atacama Large Millimeter Array. Usporedili su svoje rezultate ovisnosti ukupne količine prašine u opaženim galaksijama o količini prašine u smjeru doglednice sa poznatim rezultatima galaksija opaženih u lokalnom svemiru. Njihovi rezultati pokazuju da je dio uzorka galaksija opaženih u kontinuumu prašine konzistentan sa

opažanjima tipova galaksija u lokalnom svemiru koje imaju jako nizak stupanj formiranja novih zvijezda (eng. *quiescent*), malu količinu prašine te siromašne metalima. Ostatak galaksija neopaženih u kontinuumu prašine nalazi se ispod krivulje koja odgovara *quiescent* tipu galaksija. Nadalje, njihov rezultat pokazuje da su galaksije u uzorku, iz 1 milijarde godina starog svemira, crvenije u smjeru doglednice promatrača u usporedbi sa galaksijama u lokalnom svemiru za fiksan omjer daleko infracrvenog prema ultraljubičastom luminozitetu. No, unatoč takvom rezultatu, ipak je neobično da su galaksije neopažene u kontinuumu smještene ispod krivulje galaksija *quiescent* tipa. Takav rezultat objasnili su postojanjem mogućih grešaka u procjeni luminoziteta u infracrvenom dijelu spektra, luminoziteta u ultraljubičastom dijelu spektra koji su dobiveni iz mjerenja provedenih sa zemaljskim teleskopom UltraVISTA ili pak zbog njihove procjene parametra koji opisuje količinu prašine u smjeru doglednice promatrača koji se također temelje na UltraVISTA mjerenjima. Mogući razlog za takav rezultat mogao bi također biti i nepoznata geometrija prašine te dinamika plina koja bi mogla, po njihovom mišljenju, dati opažene rezultate.

Ipak, podatci bolje kvalitete su potrebni kako bi se provjerio njihov rezultat. Takvi podatci su upravo podatci sa *Hubble Space Telescope* Wide Field Camera 3 čije su snimke vrlo visoke rezolucije. Slike korištene u ovom radu imaju rezoluciju od 0.13 lučnih sekundi po pikselu. Osim iznimno visoke rezolucije i visoke osjetljivosti, mjerenja imaju visok omjer signala prema šumu (eng. *signal-to-noise ratio*) što omogućuje lakše raspoznavanje objekata na slici. Lakše raspoznavanje objekata ključno je u određivanju kolika je veličina aperture potrebna za dobivanje fotometrije izvora na slici, o čemu također u značajnoj mjeri ovisi kakav će biti fluks detektiranog objekta. Preciznije poznavanje fluksa vodi k preciznijim mjerenjima količine prašine u galaksiji u smjeru doglednice promatrača, odnosno ultraljubičastog spektralnog nagiba, te luminoziteta galaksije u ultraljubičastim valnim duljinama. Rezultati moje analize jasno pokazuju konzistentnost sa rezultatima prijašnjeg rada, te da odabrane *Lyman break* galaksije u uzorku u 1 milijardu godina starom svemiru doista imaju crvenije ultraljubičaste spektralne nagibe za fiksan omjer infracrvenog prema ultraljubičastom luminozitetu, u odnosu na galaksije opažene u lokalnom svemiru.

S obzirom da su rezultati mog rada konzistentni sa rezultatima prijašnjeg rada, to pokazuje da razlike između galaksija na visokom crvenom pomaku ($z > 5$) i galaksija u lokalnom svemiru nisu posljedica sistematske pogreške u mjerenjima, već doista ukazuju na drugačija fizikalna svojstva galaksija na crvenom pomaku $z > 5$, npr. drugačiju geometriju prašine, topliju prašinu ili drugačiju dinamiku plina. Luminoziteti u ultraljubičastim valnim duljinama su manji po iznosu u odnosu na ultraljubičaste luminozitete procijenjene u prijašnjem radu, stoga je omjer luminoziteta u infracrvenim i ultraljubičastim valnim duljinama veći. Taj rezultat ukazuje da promatrane galaksije imaju veću ukupnu količinu prašine nego je bilo prije opaženo. Podskup galaksija detektiranih u kontinuumu prašine su konzistentne sa opažanjima galaksija zvjezdorodnog (eng. *starburst*) tipa u lokalnom svemiru. S druge strane,

ostatak podskupa galaksija opaženih u kontinuumu prašine više su konzistentne sa krivuljom koja pripada galaksijama *quiescent* tipa opaženih u lokalnom svemiru. Galaksije ne opažene u kontinuumu ima vrlo niske omjere infracrvenog prema ultraljubičastom luminozitetu, te su smještene ispod krivulje *quiescent* tipa galaksija, ukazujući da te galaksije doista imaju drugačija svojstva plina i prašine u usporedbi sa galaksijama na nižim crvenim pomacima.

Ovakav neočekivani rezultat ukazuje na moguću prisutnost dviju različitih populacija galaksija u svemiru starom tek 1 milijardu godina. Jednu populaciju čine galaksije aktivne u formiranju novih zvijezda, bogate prašinom i metalima, te su tako po svojim svojstvima slične zvjezdorodnim galaksijama opaženim u lokalnom svemiru. Drugu populaciju čine galaksije quiescent tipa, siromašne prašinom te metalima, svojstvima nalik na Mali Mageljanov oblak opažen u lokalnom svemiru.

Kako bih provjerila koliko vrijednosti ultraljubičastih spektralnih nagiba odstupaju od stvarnih vrijednosti, izvela sam simulacije. U simulacijama sam generirala nestvarne galaksije koje sam potom umetnula u originalne slike na koordinatama na kojima nema detekcije u slikama. Nestvarne galaksije imale su nekoliko fiksiranih vrijednosti fluksa, te je svaka fiksirana vrijednost fluksa imala 1000 različitih vrijednosti ultraljubičastih spektralnih nagiba. Nakon umetanja nestvarnih galaksija u originalne slike, provela sam analizu jednaku kao i u slučaju stvarnih izvora te dobila fotometriju nestvarnih galaksija. Iz vrijednosti flukseva nestvarnih galaksija izračunala sam metodom linearne regresije vrijednosti spektralnih nagiba, te usporedila dobivene vrijednosti ultraljubičastih spektralnih nagiba sa odgovarajućim početnim vrijednostima. Iz usporedbe slijedi zaključak da dobiveni ultraljubičasti spektralni nagibi ne odstupaju značajno od očekivanih vrijednosti ultraljubičastih spektralnih nagiba, te da korekcija za vrijednosti ultraljubičastih nagiba stvarnih izvora također nije potrebna. To pokazuje dodatno da je omjer signala prema šumu kod *Hubble Space Telescope* Wide Field Camera 3 slika toliko visok da i za iznimno blijede galaksije (fluks reda veličine 10^{-19}[erg/s/cm^2/Å]) uz pravilan odabir nivoa praga šuma (eng. *threshold level*) smo u mogućnosti dobiti vrlo precizne vrijednosti fluksa te iz njih izračunati vrlo precizne vrijednosti ultraljubičastih spektralnih nagiba.

Ovi rezultati pokazuju da razlike između galaksija opaženih na niskim i visokim crvenim pomacima (z $>$ 5) nisu posljedica sistematske pogreške u mjerenjima, već drugačijih fizikalnih svojstava. Mjerenja sa *Hubble Space Telescope* Wide Field Camera 3 kao i gore navedena provjera preciznosti mjerenja pokazuju da galaksije opažene u kontinuumu na crvenom pomaku 5 $<$ z $<$ 6 pokazuju svojstva slična galaksijama na niskom crvenom pomaku. Preostali dio galaksija pokazuje vrlo niske omjere luminoziteta u infracrvenom i ultraljubičastom dijelu spektra na taj način ukazujući na moguća drugačija svojstva prašine i plina u tim galaksijama.

Proučavanjem spektara opaženih galaksija, snimljenih sa Deep Extragalactic Imaging Multi-Object Spectrograph (DEIMOS) može se ustanoviti koje od galaksija emitiraju Lyman α linije. Pomoću Lyman α linija detektiraju se galaksije aktivne u formi-

ranju novih zvijezda na niskim ali i visokim crvenim pomacima, te njihovo opažanje rezultira selekcijom široke populacije galaksija u ranom svemiru. No, njihov intenzitet značajno ovisi o količini prašine u galaksijama, s obzirom da linije mogu biti apsorbirane na zrncima prašine. Galaksije u ovom radu su klasificirane u 2 tipa na temelju detektiranog spektra, gdje prvi tip čine jaki emiteri Lyman-α linija, dok drugi tip čine galaksije koje su ili slabi Lyman-α emiteri, ili nemaju opaženu Lyman-α emisiju. Zanimljivo je pogledati položaj tih galaksija u IRX - β ravnini. Rezultat je da su jaki Lyman-α emiteri djelomično konzistentni sa krivuljom koja opisuje lokalne *quiescent* galaksije, dok su slabi Lyman-α emiteri i galaksije koje nemaju detektiranu emisiju djelomično konzistentne sa krivuljom koja opisuje lokalne zvjezdorodne galaksije. Ti rezultati bi mogli potvrditi rezultate nedavnog istraživanja provedenog na skupu galaksija na crvenom pomaku z $\sim$ 5, no kako se radi ipak o malom skupu galaksija potrebna su daljnja promatranja kako bi se mogao izvesti kvalitativan zaključak o povezanosti između Lyman-α emisije iz galaksija te njihove lokacije na IRX - β grafu.